



ΧΑΡΟΚΟΠΕΙΟ ΠΑΝΕΠΙΣΤΗΡΙΟ  
HAROKOPIO UNIVERSITY

# **HAROKOPIO UNIVERSITY OF ATHENS, GREECE**

School of Environment, Geography and Applied Economics  
Department of Geography

Master on Applied Geography and Spatial Planning,  
Sector: Geoinformatics

## **Monitoring of seasonal changes with the use of night light imaginary**

Master Thesis

**Eleni Krikigianni**  
A.M. 215309

**Athens, 2018**



ΧΑΡΟΚΟΠΕΙΟ ΠΑΝΕΠΙΣΤΗΜΙΟ  
HAROKOPIO UNIVERSITY

## **HAROKOPIO UNIVERSITY OF ATHENS, GREECE**

School of Environment, Geography and Applied Economics  
Department of Geography

Master on Applied Geography and Spatial Planning,  
Sector: Geoinformatics

### **Committee**

**Prof. Christos Chalkias (Supervisor)**  
Professor, Department of Geography, Harokopio University

**Prof Isaak Parcharidis**  
Associate Professor, Department of Geography, Harokopio University

**Prof. Dimitrios Stathakis**  
Associate Professor, Department of Planning and Regional Development  
University of Thessaly, School of Engineering, Volos

Η Κρικιγιάννη Ελένη, δηλώνω υπεύθυνα ότι:

- 1) Είμαι ο κάτοχος των πνευματικών δικαιωμάτων της πρωτότυπης αυτής εργασίας και από όσο γνωρίζω η εργασία μου δε συκοφαντεί πρόσωπα, ούτε προσβάλλει τα πνευματικά δικαιώματα τρίτων.
- 2) Αποδέχομαι ότι η ΒΚΠ μπορεί, χωρίς να αλλάξει το περιεχόμενο της εργασίας μου, να τη διαθέσει σε ηλεκτρονική μορφή μέσα από τη ψηφιακή Βιβλιοθήκη της, να την αντιγράψει σε οποιοδήποτε μέσο ή/και σε οποιοδήποτε μορφότυπο καθώς και να κρατά περισσότερα από ένα αντίγραφα για λόγους συντήρησης και ασφάλειας.

*«Years ago you told me:  
In essence, my substance is light»  
G. Seferis*

*«Εἶπες ἐδῶ καὶ χρόνια:  
Κατὰ βάθος εἶμαι ζήτημα φωτός»  
Γ. Σεφέρης*

## ACKNOWLEDGEMENTS

*This Master Thesis could not have been realized without a great deal of guidance and support of many individuals. This accomplishment would not have been possible without them.*

*It is a genuine pleasure to acknowledge my deepest sense of thanks to my supervisor **Prof. Christos Chalkias**, for his creative and comprehensive scientific advice, his meticulous scrutiny, his unwavering support and his kind supervision during my research pursuit.*

*I am also thankful to the members of the committee, **Prof. Dimitrios Stathakis** and **Prof. Isaak Parcharidis** for their valuable comments and suggestions.*

*I own a deep sense of gratitude to **Mr. Chrysovalantis Tsiakos**, for all of his love, help and encouragement throughout my research period.*

*I would like to express my gratitude to my best friend **Mr. Odysseas Kontovas**, who put his faith in me and he keeps urging me to do better.*

*Above ground, I am indebted to **my family**, whose value to me only grows by age.*

## SUMMARY

The spatio-temporal dynamics of urban development can effectively be considered as a stepping stone for urban planning, policy decision making and resource use and conservation. Consecutive satellite observations of night anthropogenic lighting and their profound study, have provide beneficial estimators of both demographic and socioeconomic dynamics. In the light of the above, the main aim of this thesis is to examine the seasonal changes in night-time satellite images, as well as their correlation with the touristic activity in EU countries. This study is conducted by using 2012 and 2013 earth observation (Night light Imaginary from DMSP (yearly basis) and VIIRS (seasonal basis) satellite programs) and statistical data associated with the touristic activity (total nights spent) in a country level (nuts 0) in Europe. These data were processed by using both remote sensing, GIS and statistical analyses (Linear regression and Geographic Weighted regression analyses). The research results show that the night-time light emissions are highly correlated with the touristic activity and that the Geographic Weighted Regression (GWR) proved to be an effective tool for the investigation of this relationship. However, a number of additional parameters should be further considered before determining the ability and the accuracy of the nightlight imaginary in the assessment of the touristic activity.

**Key words:** *DMSP, VIIRS, GIS, OLS, GWR, SOL, total night spent, tourism, Europe*

## ΠΕΡΙΛΗΨΗ

Η χωροχρονική δυναμική της αστικής ανάπτυξης μπορεί αποτελεσματικά να θεωρηθεί ως ορόσημο για τον πολεοδομικό σχεδιασμό, τη λήψη αποφάσεων και τη χρήση και διατήρηση των πόρων. Οι διαδοχικές δορυφορικές παρατηρήσεις του νυχτερινού ανθρωπογενούς φωτισμού και η βαθιά μελέτη τους, παρέχουν ευεργετικές εκτιμήσεις τόσο της δημογραφικής όσο και της κοινωνικοοικονομικής δυναμικής. Ο κύριος στόχος της παρούσας μεταπτυχιακής διπλωματικής εργασίας είναι να εξετάσει τις εποχιακές μεταβολές των δορυφορικών εικόνων νυχτερινού φωτισμού καθώς και τη συσχέτισή τους με την τουριστική δραστηριότητα στις χώρες της ΕΕ. Η μελέτη αυτή διεξάγεται χρησιμοποιώντας τις παρατηρήσεις για τα έτη 2012 και 2013 (δορυφορικά προγράμματα DMSP (ετήσια βάση) και VIIRS (εποχιακή βάση)), καθώς και στατιστικά στοιχεία που σχετίζονται με την τουριστική δραστηριότητα (συνολικές διανυκτερεύσεις) σε επίπεδο χώρας (επίπεδο 0) στην Ευρώπη. Τα δεδομένα αυτά επεξεργάστηκαν τόσο με τεχνικές τηλεπισκόπησης, όσο και με στατιστικές αναλύσεις GIS (Γραμμική παλινδρόμηση και γεωγραφική σταθμισμένη ανάλυση παλινδρόμησης). Τα αποτελέσματα της έρευνας δείχνουν ότι οι εκπομπές νυχτερινού φωτισμού συσχετίζονται σε μεγάλο βαθμό με την τουριστική δραστηριότητα και ότι η Γεωγραφική Σταθμισμένη Παλινδρόμηση (GWR) αποδείχθηκε αποτελεσματικό εργαλείο για τη διερεύνηση αυτής της σχέσης. Ωστόσο, θα πρέπει να εξεταστούν περαιτέρω ορισμένες πρόσθετες παράμετροι, πριν προσδιοριστεί η ικανότητα και η ακρίβεια των εικόνων νυχτερινού φωτισμού στην αξιολόγηση της τουριστικής δραστηριότητας.

**Λέξεις κλειδιά:** *DMSP, VIIRS, GIS, OLS, GWR, SOL, αριθμός διανυκτερεύσεων, τουρισμός, Ευρώπη*

## Table of Contents

<b>1. INTRODUCTION</b> .....	9
<b>2. NIGHT LIGHT EMISSIONS</b> .....	11
<b>2.1 OLS - Operational Linescan System</b> .....	11
<i>2.1.1 Applications of night-time imagery with DMSP-OLS</i> .....	13
<b>2.2 VIRSS - Visible Infrared Imaging Radiometer Suite</b> .....	17
<i>2.2.1 Applications of night-time imagery with VIIRS</i> .....	19
<b>2.3 Comparative analysis between OLS and VIRSS</b> .....	22
<b>3. DATA SETS &amp; STUDY AREA</b> .....	24
<b>3.1 Data sets</b> .....	24
<b>3.2 Study Area</b> .....	27
<b>4. METHODOLOGY &amp; PROCESSING</b> .....	28
<b>4.1 DMSP image processing</b> .....	28
<b>4.2 VIIRS image processing</b> .....	31
<b>4.3 Regression Analysis</b> .....	33
<i>4.3.1 Ordinary least squares regression (OLS)</i> .....	33
<i>4.3.2 Geographically Weighted regression (GWR)</i> .....	36
<b>5. RESULTS</b> .....	37
<b>5.1 DMSP regression results</b> .....	37
<b>5.2 VIIRS regression results</b> .....	41
<b>6. CONCLUDING REMARKS</b> .....	49
<b>7. LITERATURE</b> .....	50
<b>8. APPENDIXES</b> .....	57
Appendix I: Sum of Lights (SOL) for VIIRS 2012 monthly composites .....	57
Appendix II: Sum of Lights (SOL) for VIIRS 2013 monthly composites.....	58
Appendix III: Total nights spent for 2012 on a monthly basis .....	59
Appendix IV: Total nights spent for 2013 on a monthly basis .....	60
<b>9. AUTHOR INDEX</b> .....	61
<b>10. SUBJECT INDEX</b> .....	62

## Table of figures

Figure 1 Annual night-time lights composites using DMSP---OLS data, <a href="https://ngdc.noaa.gov">https://ngdc.noaa.gov</a> .....	12
Figure 2 VIIRS vs OLS in jigger fleets detection (Elvidge et al., 2015) .....	21
Figure 3 Stable lights 2012 .....	24
Figure 4 Stable lights 2013 .....	24
Figure 5 VIIRS DNB composite of December 2013 .....	25
Figure 6 Eurostat database .....	26
Figure 7 International Tourism 2016, UNWTO Tourism Highlights, 2017 Edition (Data as collected by UNWTO, July 2017).....	27
Figure 8 Steps and sub-steps of methodology .....	28
Figure 9 Projected image (left) and calibrated image (right) of 2012.....	29
Figure 10 Projected image (left) and calibrated image (right) of 2013.....	29
Figure 11 Monthly composites for April, May and June 2012 (starting from the left) .....	32
Figure 12 Forecasted monthly composites -starting from the left) for May and June 2012 .....	33
Figure 13 Linear relationship test between the studies variables.....	35
Figure 14 Regression analysis results for DMSP 2012.....	37
Figure 15 Ordinary Least Squares for SOL 2012-Residuals .....	38
Figure 16 Spatial Autocorrelation Report for DMSP 2012 .....	39
Figure 17 Regression analysis results for DMSP 2013.....	40
Figure 18 Spatial Autocorrelation Report for DMSP 2013 .....	40
Figure 19 Ordinary Least Squares for SOL 2013-Residuals .....	40
Figure 20 Regression analysis results for VIIRS Apr-Sept 2012 .....	41
Figure 21 Spatial Autocorrelation Report.....	41
Figure 22 Ordinary Least Squares for SOL 2012 (April-Sept).....	41
Figure 23 Regression analysis results for VIIRS Apr-Sept 2013 .....	42
Figure 24 Spatial Autocorrelation Report.....	42
Figure 25 Ordinary Least Squares for SOL 2013 (April-Sept).....	42
Figure 26 Regression analysis results for VIIRS Oct-Mar 2012 .....	43
Figure 27 Spatial Autocorrelation Report.....	43
Figure 28 Ordinary Least Squares for SOL 2012 (Oct-March).....	43
Figure 29 Regression analysis results for VIIRS Oct-Mar 2013 .....	44
Figure 30 Spatial Autocorrelation Report.....	44
Figure 31 Ordinary Least Squares for SOL 2013 (Oct-March).....	44

## Tables

Table 1 VIIRS Spectral Bands.....	18
Table 2: Comparative analysis between DMSP-OLS & SNPP-VIIRS (32,EL1, EL2) .....	23
Table 3 intercalibration model coefficients as calculated by Galimberti (2017) .....	29
Table 4 SOL for 2012 .....	30
Table 5 SOL for 2013 .....	31
Table 6 Max pixel values for VIIRS monthly composites for 2012 .....	31
Table 7 Max pixel values for VIIRS monthly composites for 2013 .....	32
Table 8 GWR results for April-September 2012 (left) and 2013 (right) .....	45
Table 9 GWR results for October-March 2012 (left) and 2013 (right).....	46
Table 10 Cumulative presentation of results from OLS and GWR regressions .....	47

**ABREVIASIONS**

<b>EU</b>	European Union
<b>EC</b>	European Commission
<b>EEA</b>	European Environmental Agency
<b>DGs</b>	Directorate General in EC
<b>UNWTO</b>	World Tourism Organization
<b>WB</b>	World Bank
<b>EIB</b>	European Investments Bank
<b>OECD</b>	Organization for economic co-operation and development
<b>OLS</b>	Operational Linescan System
<b>DMSP</b>	Defence Meteorological Satellite Program
<b>BRDF</b>	bi-directional reflection distribution function
<b>DN</b>	Digital Number
<b>NGDC</b>	National Geophysical Data Center
<b>NDVI</b>	Normalized difference vegetation index
<b>GDP</b>	Gross Domestic Product
<b>CO<sub>2</sub></b>	Carbon Dioxide
<b>NPP</b>	National Polar Orbiting Partnership
<b>VIIRS</b>	Visible Infrared Imaging Radiometer Suite
<b>DNB</b>	Day and Night Band
<b>vcm</b>	VIIRS cloud mask
<b>vcm<sub>sl</sub></b>	VIIRS cloud mask stray-light
<b>MIR</b>	Invariant region method
<b>SOL</b>	Sum of Lights
<b>OLS</b>	Ordinary least Squares Regression
<b>GWR</b>	Geographically Weighted Regression
<b>AIC</b>	Akaike Information Criterion

## 1. INTRODUCTION

The acquisition of socioeconomic information in various spatial scales and in an accurate and standardized way, consists a challenge for in-depth policy analysis and decision making. National and local authorities as well as the relevant EU instruments (EEA, DGs) require constant monitoring of the socioeconomic development across EU, analysis of the influence factors and forecasting of the future trends. To this end, the developments in information technology and particularly in the domain of geographic information and earth observation systems provide a valuable asset towards the acquisition of comparable data for decision making across EU.

One of the most important economic activities in European Union that also falls under the scope of this thesis is tourism. Tourism has a wide-ranging impact on economic growth, employment and social development and it is considered as one of the key counter measures in the fight against economic decline and unemployment (UNWTO, 2017). Any appraisal of its competitiveness requires a good knowledge of the volume of tourism, its characteristics, the profile of the tourist and tourism expenditure and the benefits for the European economies. Due to its importance, EU has developed an individual policy aiming others to maintain the Europe's positions as a leading tourist destination and to maximize the industry's contribution to growth and employment (EC, 2018). Various Communications have been adopted by the Commission the last decade. For instance, the communication on "A renewed EU tourism policy: towards a stronger partnership for European tourism (EC, 2006)" (COM(2006) 134 final)) pursued to address the challenges that will shape the future of the tourism sector in EU to develop more sustainable and environmentally-friendly tourism practices. The latter was followed by a set of actions in relation to the sustainable management of destinations, the integration of sustainability concerns by businesses, and the awareness of sustainability issues among tourists ('Agenda for a sustainable and competitive European tourism (EC, 2006)' (COM(2007) 621 final)). In 2010, European Commission adopted a Communication titled "Europe, the world's No 1 tourist destination — a new political framework for tourism in Europe" (EC, 2006) (COM (2010) 352 final) defining a new framework for actions to increase the competitiveness of tourism and its capacity for sustainable growth.

In addition, the Commission has developed a dedicated portal called Virtual Tourism Observatory (EC, 2018) for collecting information and conducting analysis on performance and trends in the sector. The portal provides data visualizations as maps, tables or graphs regarding: (i) the tourist demand in terms of change in arrivals accommodation establishments;

(ii) changes in the employment of the status; (iii) net occupancy rate of rooms by month; (iv) distribution of nights spent at tourist accommodation establishments; (v) arrivals and expenditure of tourists from non-EU countries to the EU28, and (vi) nights spent at tourist accommodation establishments by region. The abovementioned analysis is based mainly on data provided from Eurostat.

Tourism, can be considered as the activity of visitors to travel to a destination outside their usual environment, for less than a year. Eurostat divides tourism statistics in those relating to capacity and occupancy of collective tourist accommodation and in those relating to tourism demand. In most EU Member States, the former information is collected via surveys filled in by accommodation establishments, while the latter are mainly collected via traveler surveys at border crossings or through household surveys (Eurostat, 2017). It must be highlighted that these acquisition mechanisms involve a great deal of cost and effort and that certain countries lack such information. *Thus, at the moment there is not a streamlined modelling framework to support the calculation of tourism statistics in EU countries and regions.*

The overall goal of this master thesis is to examine the seasonal changes in the brightness of night-time satellite images, as well as their correlation with socioeconomic activities in EU countries. More specifically, the focus lies in the analysis of touristic activities and the investigation of the suitability of the abovementioned earth observation products as a proxy variable for this domain. Moreover, the proposed analysis will contribute to the study of the seasonality of touristic activities as well as the investigation/reveal of possible arisen time seasonal patterns (e.g. differences between summer and winter period).

Acknowledging the need for easily applicable, efficient, and low-cost collection of socioeconomic data, international organizations like the “World Bank” (WB), the “European Investment Bank” (EIB), and the Organization for Economic Co-operation and Development (OECD) identify the importance of the use of night-time<sup>1</sup> lights images to measure and evaluate economic development (Mukim et al., 2013).

---

<sup>1</sup> Nightlight refers to light resulting from human activity visible from outer space at night

## 2. NIGHT LIGHT EMISSIONS

### 2.1 OLS - Operational Linescan System

The Defense Meteorological Satellite Program (DMSP) was launched in the 1960s under the responsibility of the US Air Force. DMSP is engaged in the design, construction, launching and maintenance of satellites to monitor the meteorological, oceanographic and natural environment. DMSP satellites perform a sunny, almost polar track, at an altitude of 830 km from the surface of the earth and a period of 101 minutes (that is, they perform 14 rotations a day making almost universal earth coverage) (<http://ngdc.noaa.gov>).

OLS (Operational Linescan System) is a periodic scanning radiometer with the ability to display illuminated light sources in the visible and thermal infrared spectra. It is used to monitor the distribution of clouds and these temperatures twice a day. Its scanning range is 3000km and provides full daytime and night-time coverage over a 24-hour period. OLS has two broad spectral channels. The first spectral channel (VNIR) is sensitive to wavelengths of 0.4 - 1.1  $\mu\text{m}$  of electromagnetic radiation. It thus covers part of the visible and near infrared spectrum. Its radiometric capacity is 6-bit with pixel values ranging from 0 to 63. The second spectral channel records radiation in the spectral range of the thermal infrared at wavelengths of 10.0 - 13.4  $\mu\text{m}$ . Its radiometric capacity is 8-bit, that is, each pixel can receive 256 different values (from 0 to 255). Pixel values in infrared correspond to temperatures ranging from 190 to 310 Kelvin (<http://ngdc.noaa.gov>).

Like all cross-track scanning sensors, OLS uses a wide range of scanning angles to acquire images and is thus subject to two geometric problems. One has to do with the variety in reflecting a surface for a given viewing angle and lighting angle and is known as a bi-directional reflection distribution function (BRDF). Essentially, BRDF is used to describe that objects look different when viewed from different angles and when illuminated from different directions. The second problem relates to a geometric disturbance in the pixel size as the scan is removed from the nadir (Doll, 2008).

The OLS is calibrated before the launch, under conditions that resemble the space environment. Calibration data converts incoming radiation into digital values (DNs) to specific gain settings. Based on the calibration data it is possible to link the digital values with the observed radiation back to the laboratory. The gain values are modified to detect the projected illumination based on the lunar phase and elevation. In addition, a BRDF algorithm modifies the gain in the scanning portion where the illumination angle is equal to the viewing angle. Generally, gain settings gradually increase as lunar illumination decreases (Elvidge et al., 1999).

In 1992, the National Geophysical Data Center (NGDC) created a digital archive with OLS data, and since 1994 it has produced no-cloud-based global night light products based on these data. There are two ways of spatial analysis that allow data to be captured by OLS. On the one hand, we have finite data with a spatial resolution of 0.56km and on the other hand we have smoothed data with a spatial resolution of 2.7km resulting from the on-board calibration board) of full resolution data and the application of a mean value filter in each 5 x 5 cell neighborhood (Elvidge et al., 2001; Doll, 2008). This process is done to reduce the amount of memory required on the satellite (Doll, 2008). Full resolution data provides more spatial information and includes the detection of small lights that can be confused with noise in the normalized data (Elvidge et al., 2001). Today, four different types of digital satellite images are provided from the DMSP-OLS data:

- Stable lights
- Radiance Calibrated Lights
- Average Lights
- Average digital value X Percentage (Average Lights X Pct)

Stable Lights, the most widely used product of DMSP/OLS, are composite images of the mean illumination values of ground-based illumination emissions in the absence of cloud, produced annually and filtered to remove noise or other ephemeral sources (Elvidge et al., 2001). They are available on a yearly basis from year 1992 to 2012 (figure 1).

Average Visible, Stable Lights, & Cloud Free Coverages						
Year\Sat.	F10	F12	F14	F15	F16	F18
1992	F101992	-----	-----	-----	-----	-----
1993	F101993	-----	-----	-----	-----	-----
1994	F101994	F121994	-----	-----	-----	-----
1995	-----	F121995	-----	-----	-----	-----
1996	-----	F121996	-----	-----	-----	-----
1997	-----	F121997	F141997	-----	-----	-----
1998	-----	F121998	F141998	-----	-----	-----
1999	-----	F121999	F141999	-----	-----	-----
2000	-----	-----	F142000	F152000	-----	-----
2001	-----	-----	F142001	F152001	-----	-----
2002	-----	-----	F142002	F152002	-----	-----
2003	-----	-----	F142003	F152003	-----	-----
2004	-----	-----	-----	F152004	F162004	-----
2005	-----	-----	-----	F152005	F162005	-----
2006	-----	-----	-----	F152006	F162006	-----
2007	-----	-----	-----	F152007	F162007	-----
2008	-----	-----	-----	-----	F162008	-----
2009	-----	-----	-----	-----	F162009	-----
2010	-----	-----	-----	-----	-----	F182010
2011	-----	-----	-----	-----	-----	F182011
2012	-----	-----	-----	-----	-----	F182012
2013	-----	-----	-----	-----	-----	F182013

F15 2003 Nighttime Lights Composite

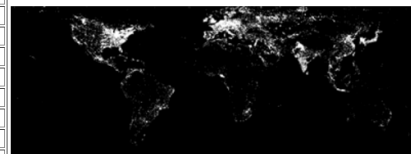


Figure 1 Annual night-time lights composites using DMSP---OLS data, <https://ngdc.noaa.gov>

They indicate the percentage frequency by which the lights are detected within a set of observations without cloud cover, but they are not a real indication of their luminosity. This is due to the fact that high values of the gain factor lead to saturation in the city lights and

consequently to the inability to derive radiation from these data (Elvidge et al., 2001). The data used to compose these images must be from the center of the OLS scanning strip, have no sunlight, moonlight, or flashes, be cloud-free, not affected by the emissions of the satellite, the gain factor is normal and the lighting in the gas burning areas is covered.

### *2.1.1 Applications of night-time imagery with DMSP-OLS*

#### ◆ Dynamic urbanization and environmental impact

The DMSP / OLS Night Lights have been used to monitor the dynamics of human settlements and measure the impact of urban development on the natural environment (Chalkias et al., 2005). In the 1970s, the OLS night visions were used to monitor the city's lights and other sources of light in the visible and near-infrared spectrum. The high contrast that characterizes OLS images, between illuminated and non-illuminated areas, allowed them to be used to identify areas where significant anthropogenic activity was taking place (Croft, 1979).

The main challenge in these applications is to distinguish permanent lighting of settlements from transient illumination and to reduce the blooming phenomenon at city boundaries, which may increase their extent (Huang et al., 2014). Imhoff et al. (1997) to address the effects of blooming and produce a more accurate map of urban areas use a thresholding algorithm. In order to separate the pixels representing urban and non-urban land use, the lower threshold gradually increased in order to find the appropriate value. However, this resulted in a non-urban area within the previously unified urban nuclei. It was generally observed that the point at which this internal fragmentation began was evident by a sudden increase in the perimeter of the studied areas. This phenomenon was used as an indicator for calculating the ideal level of the lower value for separating urban from non-urban pixels. For 3 different metropolitan areas, the levels of the lower values for which the internal fragmentation started and the mean value of them was then calculated. The average value was 89%, meaning that all pixels with  $\geq 89$  were classified as urban and all other as non-urban (Imhoff et al., 1997).

Urban area estimates were broadly consistent with baseline data. However, the negative element is that in this process many light concentrations were eliminated which represented small towns and low-density peri-urban areas. This is because these areas often have a low percentage of luminous values, usually due to recording errors. A bright pixel representing an urban area is slightly shifted from its location as it is recorded by track orbit, thus reducing the number of times assigned as a random walk. In addition, the lowest value that has emerged cannot be used for all the cities of the world, especially in developing countries where the

average light intensity is lower than the developed ones (Imhoff et al., 1997). Finally, in countries with heterogeneity in terms of level of development, a different lower value is required for each region in order to increase the accuracy of mapping (Huang et al., 2014). In general, differences in energy availability and consumption, economic growth rates and density of settlements on a regional or global scale lead to significant differences in pixel values in DMSP / OLS images (Small et al., 2005).

In other cases, other remote sensing data was used to increase the accuracy of urban mapping. Lu et al. (2008) attempted an integrated approach based on the combined use of various remote sensing data for mapping settlements in south-eastern China. The settlements were captured from Landsat ETM + images by applying a hybrid method and were the reference data. Data from DMSP-OLS and MODIS NDVI were combined, and a Human Settlement Index was developed to identify and export non-urban land coverings such as forests, farmland and water bodies. The two sets of data show differences in their characteristics. The low radiometric resolution of OLS often leads to saturation of data in urban centers and difficulty in separating different land coverings (Elvidge et al., 2007). MODIS has a higher radiometric capacity (16-bit) and provides more detailed information for segregation of land cover but cannot be used directly to map settlements due to the complexity of urban areas and the mixing of spectral signatures of the latter with those of water bodies and barren land (coverings with no vegetation). A regression model was then created for the assessment of settlements on a regional scale, in which the DMSP-OLS and MODIS NDVI data were used as independent variables and the settlements as defined by the Landsat ETM + images as a dependent variable. The result was that the combination of OLS and NDVI data provided a more accurate estimate and spatial distribution of urban settlements than would give each data separately (Lu et al., 2008).

◆ Socio-economic parameters

In addition, the correlation of night lighting data with socio-economic parameters such as population, population density, GDP and energy and electricity consumption (Elvidge et al., 2014) is strong. According to Huang et al. (2014) studies on the extraction of socioeconomic information from the night data are divided into 2 types. The first concerns the creation of a statistical relationship between night lights and the parameter considered in a geographical area, without taking into account its distribution in space. The second type of study concerns the distribution of parameters in space (Huang et al., 2014).

Sutton et al. (2001) attempted an estimate of the world population. Population estimation was based on the strong linear relationship of the surface of a city and its population, using urban concentrations as identified by OLS images of a known population. The sum of the estimated populations of these urban concentrations is the estimate of the urban population of each country. The total population of each country is calculated using published values for the proportion of the population of the country living in villages and towns of over 2,000 people (Sutton et al., 2001).

Elvidge et al. (1997) described for the first time the relationship between night lighting and economic activity at country level. Using a linear regression model, the ratio of estimated GDP (GDP) to the surface of illuminated areas, in different countries, in the fixed lights of the OLS (Elvidge et al., 1997c). Doll et al. (2000) created a global relationship of enlightened areas to GDP and created the first satellite map based on satellite data (Doll, 2008).

Understanding the distribution of wealth and the economic well-being of the population is of great importance for the implementation of policies at both European and global level. The assessment of night-time economic activity helps overcome various problems associated with data collection from surveys as they are readily available and updated at regular intervals. In addition, the shadow economy is a significant percentage of economic activity omitted from official statistics. In this context, Ghosh et al. (2010) created a model for assessing the global (including informal economy) economic activity with worldwide application, based on the OLS Night Lights. Initially, the night lights were used to calculate the sum of the light intensity values for each administrative unit and the distribution of the percentage of total economic activity not attributable to agriculture for each administrative unit. In particular, the image used has resulted from a merger of stable lights and radiance-calibrated products, which shows the luminous fluctuations in the urban centers and helps overcome the saturation problem detected in the fixed lights. Still, the use of radiometrically calibrated images contributes to the detection of dim light areas and therefore more economic activity is detected. The percentage of the total estimated economic activity attributable to agriculture for each administrative unit was spatially allocated on the basis of the Landsat population grid. A regression model was then developed to calibrate the sum of lights to predict economic activity, and unique coefficients were extracted for each administrative unit. These unique coefficients were multiplied by the sum of the headlights of each unit, thus providing estimates of total economic activity (Ghosh et al., 2010).

Sutton (1997) examines the utility of OLS night images in the spatial distribution of the population. Considering that the saturated areas of the OLS images show a strong correlation with the total population living in these areas, it attempts to model the population density within urban areas. The data used were the OLS fixed lights where the magnitude and form of urban concentrations and a 1km analysis grid with the population density of the test areas were displayed. The latter was used as a reference image for the models developed by OLS data. The relationship between the magnitude of urban concentrations and their urban population was considered logarithmic. The models used describe the population density as a function of the distance from the city center. In the center of the city the density gets its highest price. However, a deviation was observed in the models used relative to the actual population density of the reference picture. According to Sutton (1997) for a more accurate method of population density modeling it is necessary to use additional data (eg digital soil model, NDVI index etc) and lower gain levels to avoid saturation and appearance greater variance within urban concentrations (Sutton, 1997).

#### ◆ Energy

Estimation and monitoring of electricity consumption can be affected effectively by using night-time images. Moreover, the lack of electricity is an indicator of poverty and is associated with conditions detrimental to the health and well-being of people. Therefore, knowledge on electricity distribution and consumption is important for the formulation of social policies. Elvidge et al. (2010) developed a technique for estimating the population who has access to electricity based on the presence of night lights. Estimation of electricity rates was made by combining the spatial extent of night lighting and the population. Subsequently, the estimated electrification rates were compared to the published rates of the European Environment Agency (Elvidge et al., 2010). Letu et al. (2010) report that if the permanent lighting areas can be accurately derived from OLS data, it is possible to improve the accuracy of the parameters for estimating electricity consumption. Thus, a method of correction is applied using a cubic regression model to estimate the digital values of saturation light in the study area (Letu et al., 2010).

#### ◆ Other applications

A policy field in which night lights can make a significant contribution is the mapping and monitoring of greenhouse gas emissions. Some studies have been based only on the relationship between the population and CO<sub>2</sub> emissions to illustrate the spatial distribution of

the latter. (Rayner et al., 2010), while in other cases CO<sub>2</sub> emissions from point sources (eg factories) were combined with the OLS night images (Huang et al., 2014).

Night lights have been used to map and quantify light pollution. Light pollution is defined as the change in natural daylight and is created by the scattering of artificial light in the gases and small particles of the atmosphere, with a significant impact on the environment and on the health of living organisms. Therefore, modeling the distribution of night sky brightness is important for assessing its capacity for astronomical observations, quantizing of sky glow and identifying parts of the atmosphere at risk. Cinzano et al. (2001) using radiometrically calibrated night images and modeling the propagation of light into the atmosphere through the various scattering patterns created the world's first Atlas with the brightness of the night sky due to artificial light. Therefore, it has been observed that many areas which should appear dark because of the absence of terrestrial light sources have in fact been affected by light pollution from neighboring luminous areas. Moreover, comparing the above atlas with population density data, an estimate of the number of people affected was made. It was found that about 99% of the EU population and the United States and 66% of the world's population suffer some degree of light pollution (Cinzano et al., 2001).

Finally, other applications of night lights relate to the detection of night fishing vessels and fires, the assessment of the effects of gaseous emissions on the environment and on human health (Kloog et al., 2009), the impact assessment of natural disasters and military actions (Huang et al., 2014).

## **2.2 VIRSS - Visible Infrared Imaging Radiometer Suite**

Suomi National Polar-orbiting Partnership (NPP) weather satellite was first launched on October 2011 from Vandenberg Air Force Base in California. Suomi NPP passes around the earth 14 times a day (and orbits at a height of around 800 km above Earth) (Kathimerini, 2012), observing nearly the entire surface and collecting land and atmospheric data (NASA, 2014). Among the five key components that satellite was equipped with, was VIIRS (NASA, 2018). VIIRS is a scanning radiometer, which is able to collect visible and infrared images as well as radiometric measurements of land, atmosphere, cryosphere, and oceans.

VIIRS weight is approximately 275 kilograms and its average power is 200 Watt (NASA, 2018). The swath width of VIIRS is 3060 km, at a nominal satellite's altitude of 829 km. Thus, it can provide a full coverage of earth within a day. VIIRS can make use of 22 spectral bands, spatially registered (Scott, 2015), covering the wavelengths between 0.412  $\mu\text{m}$  and 12.01  $\mu\text{m}$ . Sixteen of those are moderate resolution bands (M-bands) with a spatial resolution of 750 m at

nadir, five of those are imaging resolution bands (I-bands) of 375 m at nadir, and one is panchromatic Day-Night Bands (DNB) with a 750 m spatial resolution throughout the scan (NOAA, 2013). Detailed spectral range of each band and its primary uses is presented in table 1 below.

<i>Band number</i>	<i>Spectral range (<math>\mu\text{m}</math>)</i>	<i>Primary uses</i>
M1	0.402-0.422	Ocean Color Aerosols
M2	0.436-0.454	Ocean Color Aerosols
M3	0.478-0.498	Ocean Color Aerosols
M4	0.545-0.565	Ocean Color Aerosols
I1	0.600-0.680	Imagery
M5	0.662-0.682	Ocean Color Aerosols
M6	0.739-0.754	Atmospheric Correction
I2	0.846-0.885	NDVI
M7	0.846-0.885	Ocean Color Aerosols
M8	1.230-1.25	Cloud Particle Size
M9	1.371-1.386	Cirrus/Cloud Cover
I3	1.580-1.640	Binary Snow Map
M10	1.580-1.640	Snow Fraction
M11	2.225-2.275	Clouds
I4	3.550-3.930	Cloud Imagery
M12	3.660-3.840	Sea surface temperature (SST)
M13	3.973-4.128	SST Fires
M14	8.400-8.700	Cloud Top Properties
M15	10.263-11.263	SST
I5	10.500-12.400	Cloud Imagery
M16	11.538-12.488	SST

*Table 1 VIIRS Spectral Bands*

VIIRS data are divided into three levels:

- Level 0: Raw Data Records (RDRs), which contain engineering and housekeeping data, as well as science data that are used for Level 1 data production
- Level 1: Sensor Data Records (SDRs): geolocated, calibrated radiance/reflectance and brightness temperature data, which are used as inputs to the Level 2 algorithms
- Level 2: Environmental Data Records (EDRs): are re-mapped SDRs into a Ground Track Mercator (GTM) grid (Scott, 2015).

VIIRS's imaginary can provide useful information regarding the changes in surface vegetation, land cover/land use, the hydrological cycle, and the earth's energy budget over both regional and global scales (Scott, 2015). VIIRS generates two different types of datasets. The first one is produced by NOAA and provides operational data (known as environmental data records

(EDRs)). These data are used by the National Weather Service. The second type is produced by NASA (known as Earth System Data Records (ESDRs)) and is intended to be widely used by larger scientific community for a variety of applications (e.g. Global Terrestrial Water Cycle etc.) (Wood, 2017).

VIIRS was first used to improve upon a series of measurements initiated by the Advanced Very High-Resolution Radiometer (AVHRR) sensor and the Moderate Resolution Imaging Spectroradiometer sensor (MODIS). MODIS and AVHRR radiometric measurements, provide knowledge on the dynamics of different geophysical phenomena, including: aerosol and cloud properties, sea, land and ice surface temperatures, ice motion, fires, and the albedo of Earth. On the other hand, VIIR's mission, is focused on the monitoring of changes and properties in vegetation, land cover/use, the hydrologic cycle, and the earth's energy budget over both global and regional scales. The combination of the data of the three aforementioned sensors, will effectively provide scientists, in the next few years, with a thorough assessment on the climate change effects on earth over the last 20 years (Scott, 2015).

VIIRS can be mainly used to monitor cyclical changes caused by human activities such as holiday lighting and seasonal migrations. They can also be used as a tool for monitoring gradual changes occurred by urbanization, out-migration, economic changes, and electrification (Carlowicz, 2017).

### *2.2.1 Applications of night-time imagery with VIIRS*

#### ◆ Estimation of socioeconomic variables

Most of the applications of VIIRS DNB images for the estimation of socioeconomic variables aim on the one hand to examine the capabilities of the new-generation night-time lights image products in estimating economy and on the other hand to establish their improved accuracy over DMSP/OLS.

Various studies have emerged since the availability of the first annual products of VIIRS, investigating the potential of VIIRS imagery in modelling socioeconomic parameters in various scales. Shi et al. (2014a) implemented a series of geo-processing routines to eliminate background noise and remove outliers from VIIRS night-time data so as to estimate the Gross Domestic Product and the Electric Power Consumption of China. In particular, they used DMSP/OLS data to generate a mask with all pixels with positive DN values. Based on this mask an initial corrected image of VIIRS data was extracted, relieved from ephemeral lights and background noise. Then, a low pass filter was applied to remove existing outliers in the

image. Pixel values exceeding a particular threshold, were assigned with a new value based on the maximum DN value within their immediate 8 neighbors. Finally, a linear regression was undertaken yielding a greater correlation with the estimated factors than DMSP data (Shi et al., 2014a). In the same wavelength, Jing et al. (2016) calculated the correlation between VIIRS night-time data indexes and 12 socioeconomic variables. In this case, the removal of background noise was achieved via the use of threshold values derived from object functions (optimal threshold method). Pixel values exceeding the threshold were assigned with 0 (Jing et al., 2016).

Zhao et al. (2017) examined the efficiency of monthly VIIRS DNB images in the calculation of GDP in the USA. Their data processing methodology included the implementation of a python-based exponential smoothing algorithm that aims to tackle the problem of missing data in high-latitude regions of the northern hemisphere in the summer. This computational technique consists of two basic functions of forecasting and smoothing time series data. Following the processing method, the logarithms of sum radiance were extracted from the DNB images and were regressed with the logarithm of GDP at country level. A linear regression was applied due to its higher accuracy, demonstrated in the literature. In addition, the performed logarithmic transformations aimed to make distributions of the data less skewed and to further improve accuracy (Zhao et al., 2017).

#### ◆ Mapping global fossil fuel carbon dioxide (CO<sub>2</sub>) emissions

CO<sub>2</sub> is a greenhouse gas product produced mainly by anthropogenic activities. Communities and policy makers make enormous efforts in creating inventories leading to emission reduction. Based on its higher spatial resolution and the wider radiometric detection range, than the traditional DMSP-OLS night-time light data, VIIRS can be used as a very useful and reliable data source for the assessment and distribution of the CO<sub>2</sub> emissions. A pool of studies (Elvidge et al. (2001), Doll et al. (2000), Raupach et al. (2010), Meng et al. (2014), Su et al. (2014), Shi et al. (2016)) has shown the correlation between CO<sub>2</sub> emissions and the light area, the average values of night light, and the total amount of lights within a given area respectively (Zhang et al., 2017). Ou et al. (2015) through a comparative analysis of NPP-VIIRS, RCP-DMSP-OLS, SLP-DMSP-OLS data and data of land cover, concluded that NPP-VIIRS data have a better spatial variation of CO<sub>2</sub> emission, although there is a two-year gap between the NPP-VIIRS data and land cover dataset (Ou et al., 2015). However, the characterization effects at different spatial scales were not considered. On the other hand, Zhang et al. (2017) state that DMSP-OLS is more accurate than NPP-VIIRS in modeling CO<sub>2</sub> emissions, considering also both the

accuracy of the gridded CO<sub>2</sub> emissions and the corrected datasets of the aforementioned sensors.

◆ Monitoring jigger fleets

A variety of literature can be used to demonstrate the representative use of satellite images to monitor jigger fleets. Elvidge et al. (2010) mention that the DMSP-OLS images have been widely used to indicate the movements of fleets. Cozzolino & Lasta (2016), proved that VIIRS Day-Night Band pixel footprint, although it is bigger than the length of vessel (50–60 m) pixel, can effectively identify and estimate the positions of the jigger ships. In addition, Saitoh et al. (2010), conclude that it is possible to estimate the number of vessels using remotely sensed night-time images. Elvidge et al. (2015), through a comparative analysis between OLS and VIIRS day/night band (DNB) refer to the fact that VIIRS collect imaging data with 45 times smaller pixel footprint than the OLS (figure 2).

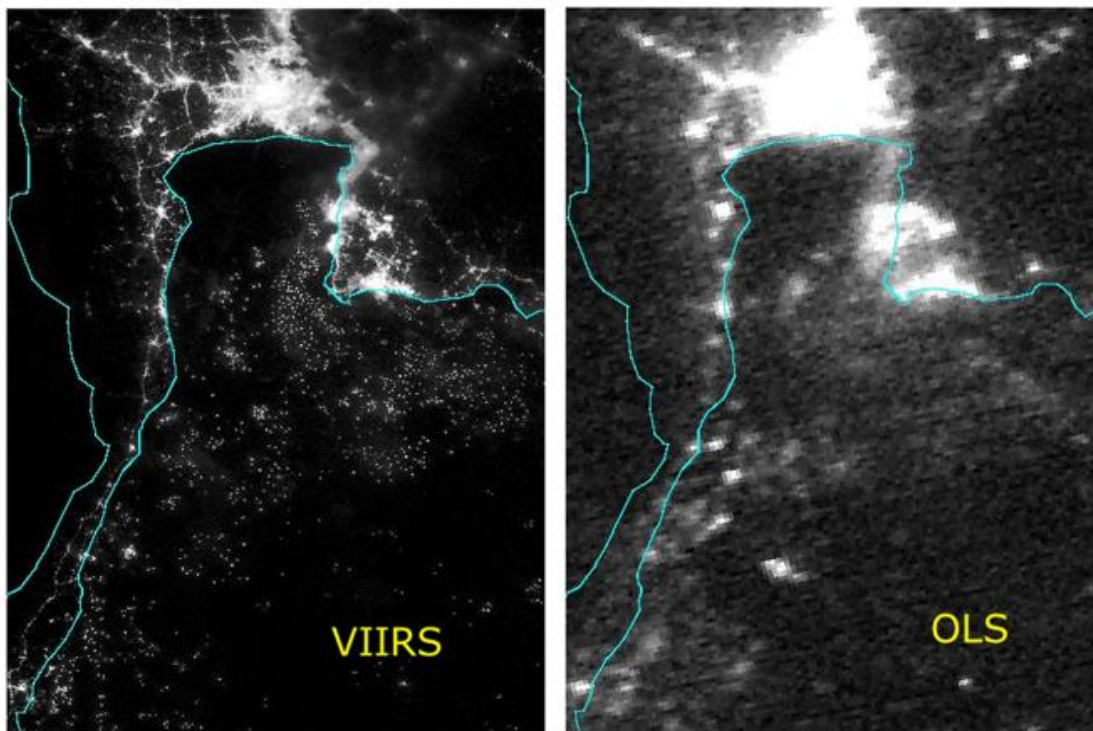


*Figure 2 VIIRS vs OLS in jigger fleets detection (Elvidge et al., 2015)*

◆ Gas flares

Elvidge et al. (2016) made use of VIIRS data to detect and measure radiant emissions from gas flares in a global scale, by collecting the shortwave and near-infrared data at night, and simultaneously recording the peak radiant emissions from flares. According to Elvidge et al. 2013, VIIRS M10 spectral channel records among others, also gas flares, based on their anomalies in pixels' values.

As flare operators lack of having established a systematic reporting, satellite imagery/sensors are a tempting solution for monitoring gas flares in a global scale (Elvidge et al. 2015).

◆ Stock of buildings and civil engineering infrastructures

Night light images can be widely applied in optimizing the urban planning process. Hsu et al. (2011, 2013) proved that DMSP-OLS RC NTL can provide a good estimation of in-use steel stock of buildings and civil engineering infrastructure at prefecture and national levels. Also, Hattori et al. (2013) monitored the continuous change of the in-use steel stock in buildings and civil engineering infrastructure. Based on the VIIRS release in 2013, Shi et al. (2014a), reported that VIIRS can be used as a good proxy for extracting urban built-up areas. Hanwei et al. (2016), concluded that urban night-time lights are more reliable for estimating in-use steel stock in buildings whereas total night-time lights are more accurate in modeling in-use steel stock civil engineering infrastructure. Additionally, it was proved that VIIRS data had stronger relationships with both buildings and civil engineering infrastructures than DMSP-OLS data.

### **2.3 Comparative analysis between OLS and VIIRS**

In this sub-chapter a comparative analysis between DMSP-OLS and SNPP-VIIRS sensor and images is presented (table 2). This analysis will facilitate the process of interpreting the results of the current study. Given this, table 2 summarizes the characteristics of the two systems, their similarities and their differences. To start with their common characteristics, these are stipulated in their similar polar orbits, the same wide swath (3000 km) and their similar band passes for the low light imaging band (0.5 to 0.9  $\mu\text{m}$ ).

Like all new technological releases, VIIRS appears to be more advantageous than DMSP with advanced capabilities. It provided ground footprint at 742m (15 arc-second, about 500 m), a 14-bit dynamic range and it has a calibrated radiometer. OLS has a spatial resolution of 2.7km (with 45 times bigger footprint) (30 arc-second, about 1000 m), with a 6-bit dynamic range and lacks of onboard calibration (8)+ (3). In addition, VIIRS products have been improved because of the existence of a wider radiometric detection range, which can effectively deal with the saturation problem of DMSP-OLS in urban cores (31). VIIRS contains, also, 21 additional spectral bands, with the ability to differentiate lights from other luminous sources and to the optical thickness of clouds.

Another significant difference of the two systems is the overpass time. VIIRS overpasses around 1.30 a.m, while DMPS passes around 7.30 p.m. This can be considered as a difficulty for VIIRS, as peak lighting for urban areas usually occurs during the afternoon hours and before

10.00 p.m., with a gradual minimization of their outdoor lighting, after that time, Nevertheless, it has been examined, that VIIRS Day and Night band can detect lights even after midnight (32).

To sup up, the substantial improvements of VIIRS images over the OLS can be outlined to their higher level of quantization, their rigorous calibration, and the existences of additional spectral bands useful for cloud, ocean and combustion source characterization (Elvidge, 2015). Nevertheless, it is also worth to mentioned that VIIRS images are characterized by two significant limitations: The first one refers to their short timeseries (from 2012), compared to the DMSP (from 1992), and the second one to the fact that a significant number of images are affected by stray-light, leading to missing data for a couple of months (depending on the area).

	Variable	DMSP-OLS	SNPP-VIIRS
	Timeseries Availability	From 1992-2018	From 2012-Present
	Orbit	Sun-synchronous-Polar-850km altitude, 98.8 degree inclination, 102 minutes	Sun-synchronous-Polar-827km altitude, 98.7 degree inclination, 102 minutes
	Swath	3000km	3000km
	Low light imaging bandpass	Panchromatic 0.5 to 0.9 um	Panchromatic 0.5 to 0.9 um
<b>DIFFERENCES</b>	Night time overpass	~19:30	~01:30
	Builder/Operator	U.S. Air Force	NASA-NOAA Joint Polar Satellite System (JPSS)
	Ground footprint	5km x 5km at nadir	742 m x742 m
	Spatial resolution	2.7km	750m
	Additional Spectral bands	Two spectral bands (vis and TIR)-Thermal infrared (10um)	21 additional bands spanning (11 at night / 21 at day) 0.4 to 13 um
	Quantization	6 bit	14 bit
	Saturation	Common in urban cores	No saturation
	Calibration	None for low light imaging band	On board Solar diffuser used to calibrate daytime DNB data. Calibration is extended also to low light imaging mode

Table 2: Comparative analysis between DMSP-OLS & SNPP-VIIRS (32,ELI, EL2)

### 3. DATA SETS & STUDY AREA

#### 3.1 Data sets

##### 3.1.1 *DMSP night time imagery*

DMSP nightlight images, were accessed through the National Oceanic and Atmospheric Administration website on 1st of April 2017. The two selected images (for years 2012 and 2013 respectively) (figures 3 & 4) concern the average visible, stable lights, & Cloud Free Coverages. The pixel values of the cloud free coverage composites represent the total number of observation that were reordered for each pixel during a calendar year. The pixel value has 6 bit radiometric quantification levels, with a range between 0 (no light) and 63 (Wei et al., 2014). The stable light image composites were produced by making a further cleaning up of the ephemeral light sources (e.g. fires, fishing boats etc). Their characteristics are referring to: cloud-free composites, 30 arc second grids (approximately 1km), -180 to 180 degrees longitude and -65 to 75 degrees latitude. In particular, the 2012 & 2013 DMPS stable light images are provided by the F18 satellite program, which will run until 2018 (OSCAR, 2018).



Figure 3 Stable lights 2012



Figure 4 Stable lights 2013

##### 3.1.2 *VIIRS night time imagery*

By accessing the National Oceanic and Atmospheric Administration website, the 24 monthly images (covering the period from January 2012 to December 2013), of version 1 of the night-time VIIRS Day and Night band (DNB), cloud free composites (figure 5), Tile 2 (75N/180W TO 0N/60W/) covering almost the entire Europe, were downloaded on 10th of April 2017. The images are produced in 15 arc-second geographic grids.

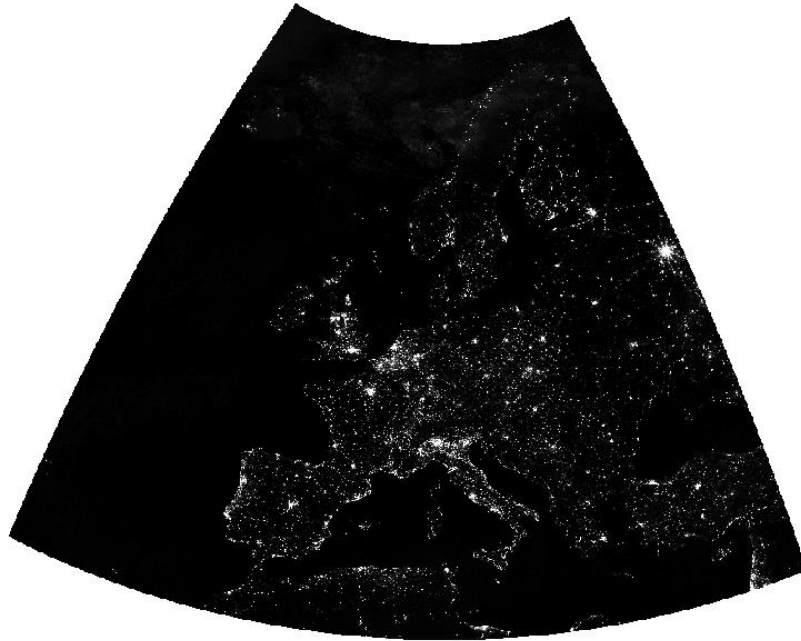


Figure 5 VIIRS DNB composite of December 2013

Each tile is actually a set of images containing average radiance values and numbers of available observations. DNB monthly composites are available in two different configurations: The first excludes any data impacted by stray light (denoted as “vcm”), whilst the second includes these data if the radiance values have undergone the stray-light correction procedure (denoted as “vcmsl”).

Due to the reduced quality of the “vcmsl” version, the first configuration was used in order to achieve better results in our seasonal monitoring application.

### 3.1.3 *Statistical data*

Statistical information used for this study, were acquired by *The Eurostat Dissemination Database*, which provides official statistics for the European Union, EU member states and sub-state regions (nuts 0, nuts 1, nuts 2 & nuts 3) (Eurostat, 2013). Among the nine primary categories (figure 6), we made use of the available variable regarding the «*Nights spent at tourist accommodation establishments by residents/non-residents (tin 00171)- Total nights spent*», in nuts 0 level (country level), on a monthly basis, for the years 2012 & 2013 respectively (figure 6) (Eurostat 2018). Thus, we assume that ‘total nights spent’ value is a reliable index of ‘touristic activity’ at national scale. The monthly freely available data, were easily used both in their correlation on a yearly basis with the Sum of Lights (SOL) from DMSP images and on a seasonal 6-month basis with the SOL from VIIRS.

It must be also taken into consideration that the aforementioned statistical data are affected by tax evasion (establishment which do not declare the real number of stays) and by current accommodation trends (such as Airbnb, couch-surfing,) which do not make their data publicly available (Stathakis et al.,2017)

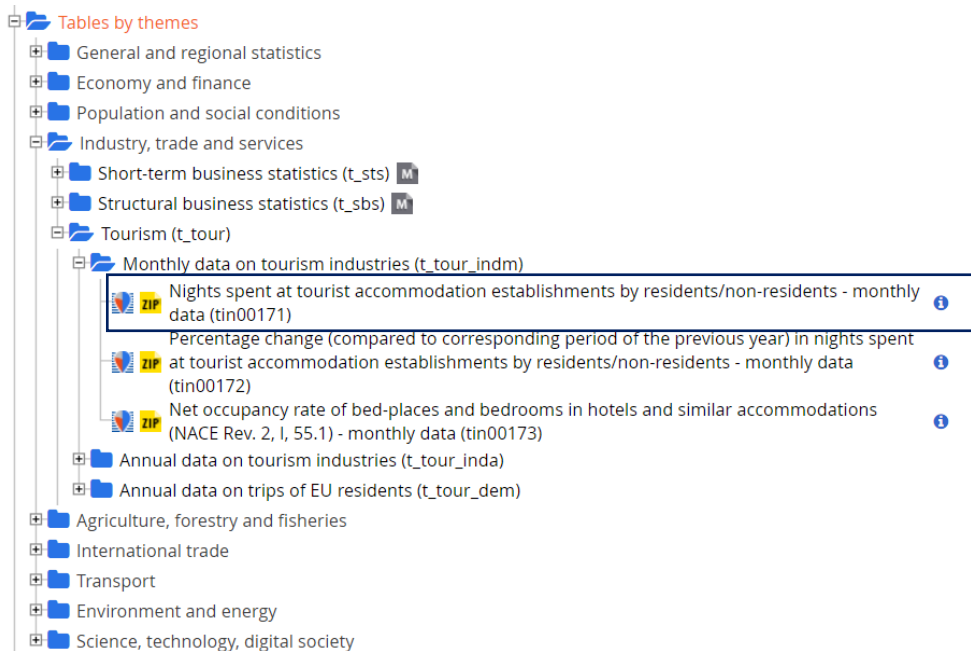


Figure 6 Eurostat database

The Eurostat interface<sup>2</sup> provided us with a specific selection of the data due our predefined spatial, time and unit of measurement constraints (Statistical data used for this study are available in appendix III and IV). In terms of the time constraints and given the fact that selected DMSP images are referring to 2012 and 2013, the statistical data were obtained accordingly. As for the spatial constraints, for four out of thirty-six countries (namely Switzerland, Ireland, Turkey and Former Yugoslan Republic of Macedonia) no data were reordered for the years 2012 and 2013. Last but not least, as unit of measurement for the aforementioned variable *-Total nights spent-* has been decided, the integral number of measurements.

<sup>2</sup> [http://appsso.eurostat.ec.europa.eu/nui/show.do?dataset=tour\\_occ\\_nim&lang=en](http://appsso.eurostat.ec.europa.eu/nui/show.do?dataset=tour_occ_nim&lang=en)

### 3.2 Study Area

According to European commission (Eurostat, 2013), Europe is considered as a prominent tourist destination and world's most visited region, holding approximately a 49% share of the global tourist arrivals in 2016 (UNWTO, 2017) (figure 7).



Figure 7 International Tourism 2016, UNWTO Tourism Highlights, 2017 Edition (Data as collected by UNWTO, July 2017)

Given also the fact that tourism, except for its operation as an engine of economic prosperity is considered as a significant source of employment -especially in the Mediterranean region (EC, 2001)- and its rapid growth during the last fifteen years (Stevenson et al., 2008), its study through the use of satellite products and its consideration as a proxy variable can provide policy makers and tourism industry with a comparative advantage in the way of defining new sustainable strategies.

#### 4. METHODOLOGY & PROCESSING

In this study a three-step methodology is applied, for examining the seasonal changes in night images and their correlation with the touristic activity. The first and second step, comprises a sequence of image-processing analyses of DMSP and VIIRS images respectively, leading to the extraction of the SOL index. The third step is related to the statistical analysis, using the linear and the Geographically Weighted regression (GWR). The steps are illustrated in figure 8 below and are thoroughly described in the following sections.

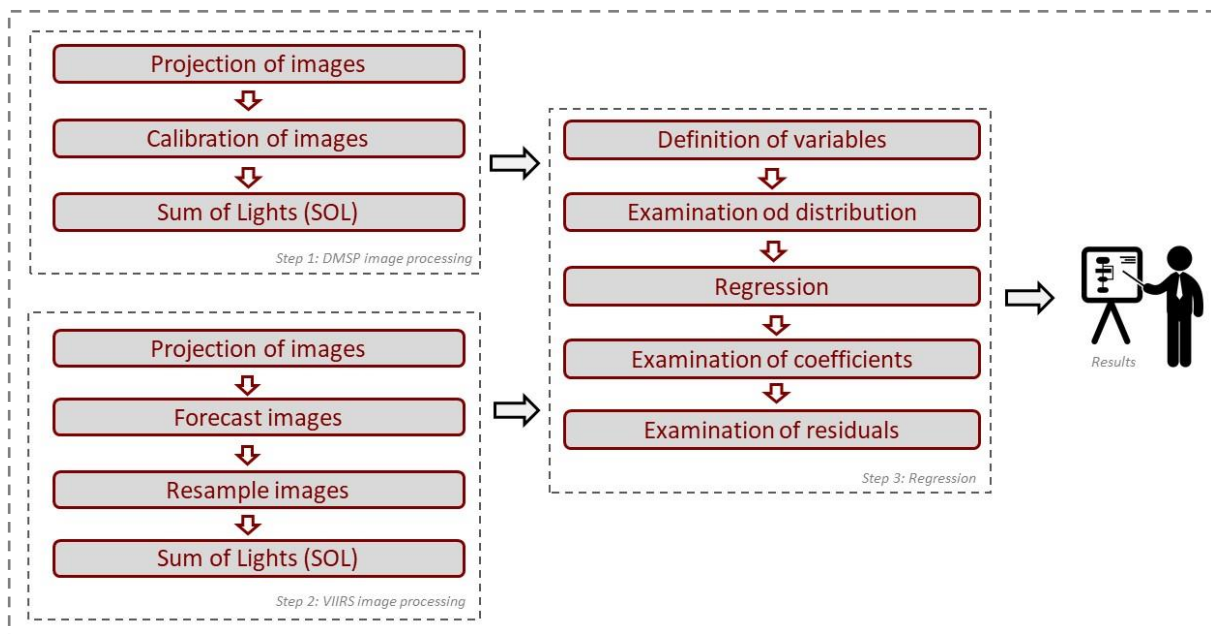


Figure 8 Steps and sub-steps of methodology

##### 4.1 DMSP image processing

By making use of ArcGIS software, the original 2012 and 2013 DMSP input images were projected from the World Geodetic System (WGS84) (EPSG: 4326) to Lambert azimuthal equal-area (ETRS89-LAEA Europe) (EPSG: 3035). LAEA projection maintains the area of polygons while simultaneously maintaining the direction from the centre. By being projected in LAEA, the two datasets accurately represent the area in all regions of the sphere and the impact of area distortion is eliminated.

On a year to year basis, the sensor degradation, causes changes in the OLS satellite's performance (e.g. differences in sensor calibration, in acquisition times etc.) (Zhang and Seto, 2011). These measurement errors can be reduced, by applying one of the two existing methods: the 'Invariant region method (MIR)' -most applied by remote sensing researchers- (Elvidge et al., 2009) and the 'year fixed effects -most applied by economists- (Henderson et al. 2012). In this study we made use of the former method -MIR- by selecting Sicily as the invariant region

and the F152006 as the reference imagery. The intercalibration model coefficients of each image have been calculated by Galimberti (2017) by using a second order polynomial regression model and are stipulated in the table 3 below:

Image	C <sub>0</sub>	C <sub>1</sub>	C <sub>2</sub>	R <sup>2</sup>
F182012	1.6511	0.3815	0.0078	0.954
F182013	1.5803	0.4479	0.0064	0.957

Table 3 intercalibration model coefficients as calculated by Galimberti (2017)

After the coefficients are figured out, a new second order polynomial model is performed, to find the new Image values for calibrated image:

$$\text{Image}_{\text{calibrated}} = C_2 * \text{Image}^2 + C_1 * \text{Image} + C_0$$

The figures below (9 and 10), stipulate the projected (on the left) and the calibrated (on the right) images of the years 2012 and 2013 respectively:

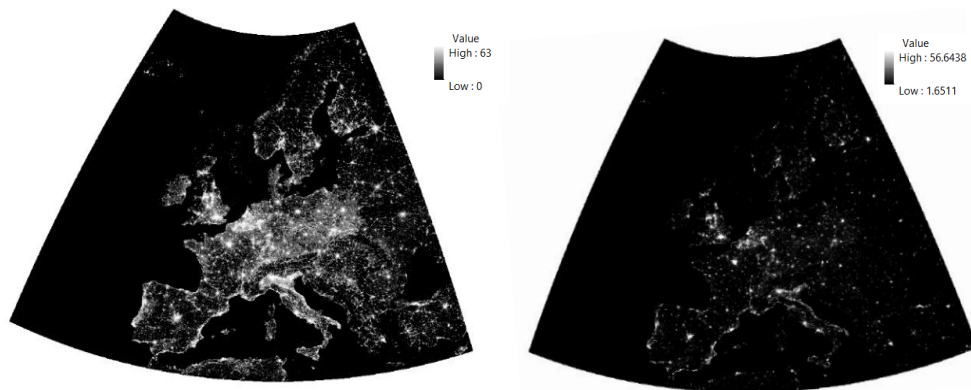


Figure 9 Projected image (left) and calibrated image (right) of 2012

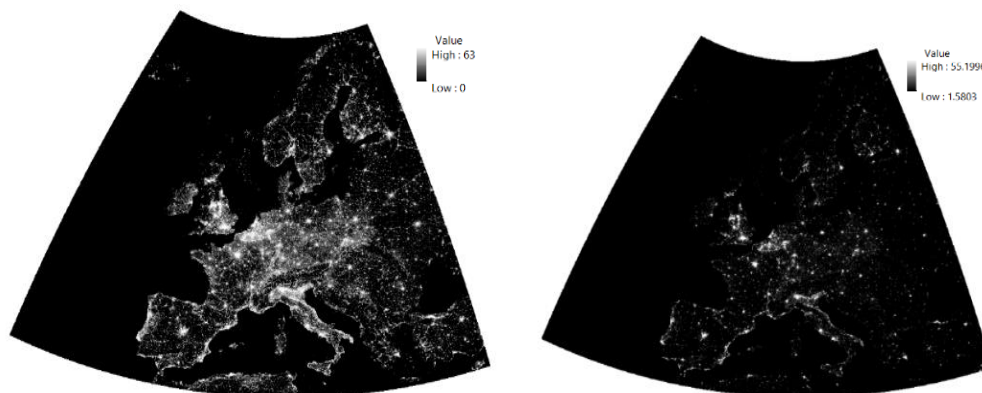


Figure 10 Projected image (left) and calibrated image (right) of 2013

As indicating from the values of the images, DMSP-OLS night time images, consists of many pixels with very low and zero values ( $DN < 6$ ) and at the same time with many pixels with saturated values ( $DN > 63$ ). Saturated values don't represent ground luminosity and low DN doesn't provide surface information. Thus, in order to avoid both the blooming effect and the light saturation problem, the Digital Number (DN) values of the calibrated images must be based on the 6-bit (0-63) quantization. Thus, zero value pixels and pixels with a significant lower value ( $DN < 6$ ) are discarded and blooming effect is removed and brightest pixels ( $DN = 63$ ) are removed and saturation problem is resolved. Given this, the threshold for the lowest value has been set to zero and for the highest to 63, by using the following expression for each of the two calibrated images:

$$\text{Con}(\text{Image} < 6, 0, \text{Image})$$

$$\text{Con}(\text{Image} > 63, 63, \text{Image})$$

Hereupon, we continue by calculating the Sum of lights (SOL) within the zones of European Countries (nuts 0 level). SOL indicator is the sum of all DN values in an area (Stathakis, 2016). SOL is calculated per country, by using zonal statistics and the results are shown in the tables 4 & 5 below:

Country Abbreviation	Sum of Lights	Country Abbreviation	Sum of Lights
<b>AT</b>	285315.8	<b>LI</b>	2289.385
<b>BE</b>	675599.5	<b>LT</b>	76205.34
<b>BG</b>	88378	<b>LU</b>	34192.49
<b>CY</b>	66225.4	<b>LV</b>	51029.13
<b>CZ</b>	451480.4	<b>ME</b>	14088.38
<b>DE</b>	2352807	<b>MT</b>	15411.82
<b>DK</b>	195636.5	<b>NL</b>	621148.8
<b>EE</b>	71921.28	<b>NO</b>	538174.6
<b>EL</b>	389239	<b>PL</b>	1422671
<b>ES</b>	2308900	<b>PT</b>	628996.8
<b>FI</b>	888153.2	<b>RO</b>	232275.2
<b>FR</b>	2832995	<b>SE</b>	911702.5
<b>HR</b>	157098.1	<b>SI</b>	74549.86
<b>HU</b>	208559	<b>SK</b>	131175.5
<b>IS</b>	36035.4	<b>UK</b>	2247102
<b>IT</b>	3220958		

*Table 4 SOL for 2012*

Country Abbreviation	Sum of Lights	Country Abbreviation	Sum of Lights
<b>AT</b>	316556.3	<b>LI</b>	2396.125
<b>BE</b>	694465.1	<b>LT</b>	81948.17
<b>BG</b>	97309.76	<b>LU</b>	36690.3
<b>CY</b>	69564.05	<b>LV</b>	54830.51
<b>CZ</b>	501561.3	<b>ME</b>	15559.29
<b>DE</b>	2547412	<b>MT</b>	15302.04
<b>DK</b>	214098	<b>NL</b>	646985.7
<b>EE</b>	77486.13	<b>NO</b>	584898.8
<b>EL</b>	418062.9	<b>PL</b>	1579001
<b>ES</b>	2410410	<b>PT</b>	657387.6
<b>FI</b>	949298.5	<b>RO</b>	253390.2
<b>FR</b>	3031921	<b>SE</b>	994253.8
<b>HR</b>	174096.3	<b>SI</b>	83267.77
<b>HU</b>	228486.1	<b>SK</b>	146872
<b>IS</b>	39414.31	<b>UK</b>	2330048
<b>IT</b>	3381371		

Table 5 SOL for 2013

#### 4.2 VIIRS image processing

Images were projected from the World Geodetic System (WGS84) (EPSG: 4326) to Lambert azimuthal equal-area (ETRS89-LAEA Europe) (EPSG: 3035) in ArcGIS software. The original NPP-VIIRS imagery (unlike DMSP-OLS data) contains lights detections associated with cities, transportation corridors, gas flares, fires, background noise, volcanoes, aurora and in some cases lights which are associated with the reflectance of light off bright surfaces, such as snow-covered mountains or bright lakes (Li et al, 2013 & Kaifang et al., 2014). For removing the confounding factors and according to Xin et al. (2015), the five most developed administrative regions in nuts 2 level in Europe (namely United Kindom (UKI3), Denmark (DE30), Spain (SP30), Italy (ITI4) and France (FR10)) have been chosen, and their maximum pixel values on a monthly basis (tables 6 and 7) have been obtained.

Nuts 2 areas	Apr	May	June	July	Aug	Sept	Oct	Nov	Dec
UKI3	0	0	0	0	0	195.27	314.35	186.96	<b>314.27</b>
DE30	0	0	0	0	0	250.75	109	168.23	123.29
ES30	<b>218.12</b>	0	0	0	172.08	20.67	<b>413.27</b>	<b>307.42</b>	313.19
ITI4	181.39	0	0	0	<b>703.9</b>	186.57	195.72	187.36	286.47
FR10	0	0	0	0	0	<b>264.44</b>	202.49	223.72	265.72

Table 6 Max pixel values for VIIRS monthly composites for 2012

Nuts 2 areas	Jan	Feb	Mar	Apr	May	June	July	Aug	Sept	Oct	Nov	Dec
UKI3	92.78	258.46	<b>245.98</b>	161.43	0	0	0	0	121.10	143.31	313.62	202.35
DE30	39.31	96.08	160.02	0	0	0	0	0	0	145.17	74.07	126.06
ES30	176.70	240.93	193.93	212.76	<b>454.70</b>	0	0	181.73	196.5	<b>351.40</b>	217.92	<b>334.84</b>
ITI4	182.02	226.16	147.18	199.56	0	0	0	<b>196.21</b>	171.03	184.22	206.88	208.22
FR10	<b>259.88</b>	<b>321.85</b>	225.55	<b>230.82</b>	0	0	0	0	<b>228.36</b>	203.14	<b>515.55</b>	250.28

Table 7 Max pixel values for VIIRS monthly composites for 2013

The hypothesis of this methodology is that other areas should not exceed the pixel values of the aforementioned five regions theoretically. Given this, the threshold for the highest value has been set to the maximum value for each month, as indicated (in red) in tables 6 & 7, by using the following expression for each image:

$$\text{Con}(\text{Image} > \text{max value}, \text{max value}, \text{Image})$$

Continuing with the VIIRS image processing, it is of utmost importance to mention that VIIRS DNB composites for April, May, June, July, August and September, contain pixels with no data, because of the solar illumination which affects the northern regions in summer (figure 11) (Zhao, 2017).

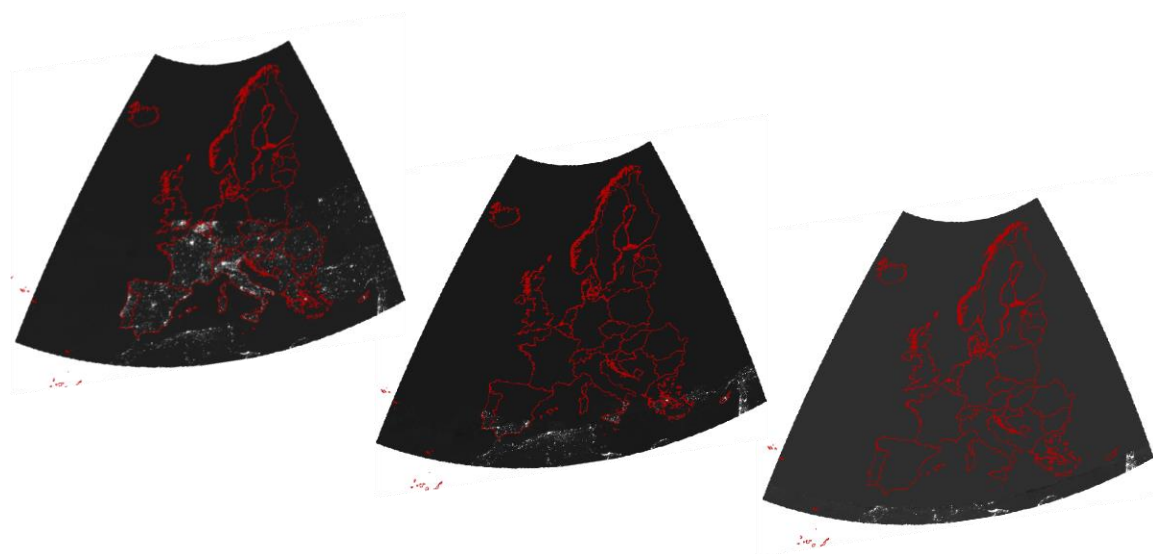


Figure 11 Monthly composites for April, May and June 2012 (starting from the left)

To attend this matter, the technique of exponential smoothing (Zhao, 2017) has been applied for smoothing and forecasting time series data, by using an algorithm (in R studio) where a new forecasted composite is produced with a temporal proximity of two months of the existing composites. As new composites have a different cell size, the Nearest Resampling technique was used and the cell size (X,Y) was set to the one of existing rasters (October to March), namely, 436\*436. The new produced composites were constituted both from the new

forecasted pixel values and the existing ones- where available- by using raster mosaic technique (Mosaic to new raster) of ArcGIS software (figure 12).

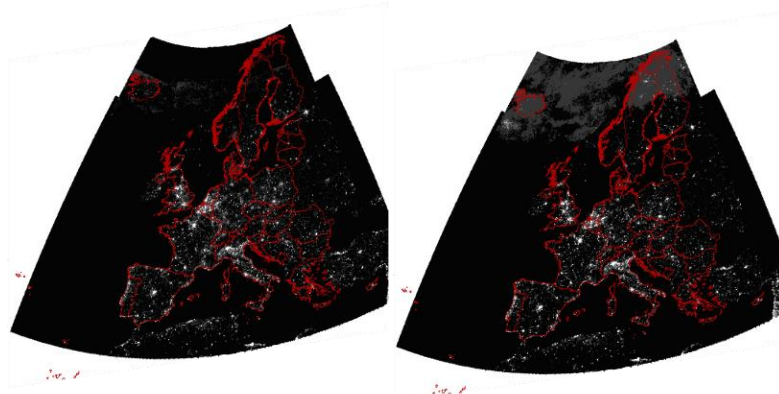


Figure 12 Forecasted monthly composites -starting from the left) for May and June 2012

Finally, we continue by calculating the Sum of lights (SOL) index (Elvidge et al., 2014) within the zones of European Countries (nuts 0 level). SOL is calculated per country, by using zonal statistics and the results are shown in Appendix 1 & 2.

### 4.3 Regression Analysis

#### 4.3.1 Ordinary least squares regression (OLS)

Exploring the possibility of using nightlight imagery as a proxy for monitoring tourism activities, demands the implementation of regression models that will establish the relationship between SOL index and the variables under investigation. Regression analyses attempt to show the degree to which one or more variables can potentially cause positive or negative change in another variable (Murack, 2013). Regression analysis supports modelling, examination and exploration of relationships as well as interpreting the factors behind observed patterns. Linear regression consists on the most widely known types of regression analysis.

A linear regression analysis yields a mathematical equation (linear model) that estimates a dependent variable Y from a set of predictor variables or regressors X. The following equation presents the most general form of a linear model (Darlington & Hayes 2017):

$$Y=b_0+b_1X_1+b_2X_2+\dots+ b_kX_k+e$$

Where Y is the dependent variable that we are trying to predict or understand (in our case the total nights spent); X is the independent variable of the model (the SOL index);  $b_0$  is the regression constant (also called Y-intercept); b are the regression coefficients or simply the regression weight that determines how much the equation uses values on that variable to produce an estimate of Y; e is the random error (residuals) that indicates the unexplained portion of the dependent variable.

Since the derivation of the regression equation is based on minimizing the sum of the squared residuals, this method is called ordinary least squares regression or just OLS regression. In OLS regression, the distribution's spread is measured via the standard deviation, whilst the correlation between X and Y is calculated via the Pearson correlation coefficient. The Pearson correlation coefficient, or simply the correlation, between X and Y is defined as the covariance of X and Y divided by the product of their standard deviations.

$$r_{xy} = \text{Cov}(XY) / S_x S_y$$

Pearson correlation measures the strength of the association between X and Y. If the coefficient is equal to 1 or -1, there is perfect linear association between X and Y, whereas if the coefficient is equal to 0, X and Y are linearly independent. The sign of the coefficient conveys the direction of association. Positive values of the coefficient, indicate that cases above the mean on X tend to be above the mean on Y, and cases below the mean on X tend to be below the mean on Y. When Pearson coefficient is negative, cases above the mean on one variable tend to be below the mean on the other. Since a variance is a type of covariance and a standard deviation is the square root of a variance, Pearson correlation coefficient shows that a correlation is determined entirely by covariances (Darlington & Hayes 2017). In this study, Pearson correlation (r) is presented in figure 13.

In this study, a cross sectional (linear) regression analysis has been applied two times. The first one, for defining the correlation between the SOL of DMSP images and the variable of 'total nights spent in a place' on an annual basis (for two years namely, 2012 & 2013), while the second one applied for defining the correlation between the SOL of VIIRS images and the variable of 'total nights spent in a place', on a seasonal basis -for the years 2012 and 2013- and more specifically between the summer (April to September) and winter (October to March) period.

Before the analysis of the data, part of the process was to make sure that the data we want to analyse can actually be analysed by using linear regression. A set of assumptions have been taken into account and the way we tackled the issues is presented below:

***Assumption 1: A linear relationship between the two variables is needed***

By using IBM SPSS Statistics software, a scatterplot has been created. The dependent variable (total nights spent in a place) has been tested against the independent variable (SOL of DMSP 2012 and SOL of DMSP 2013, as well as with SOL of VIIRS 2012 (1<sup>st</sup> and 2<sup>nd</sup> semester) and SOL of VIIRS 2013 (1st and 2nd semester)). The six produced scatterplots, showed the

existence of linearity (figure 13) and the outcome of Person Correlation ( $r$ ), which indicates the satisfactory and very strong linear correlation of the examined variables.

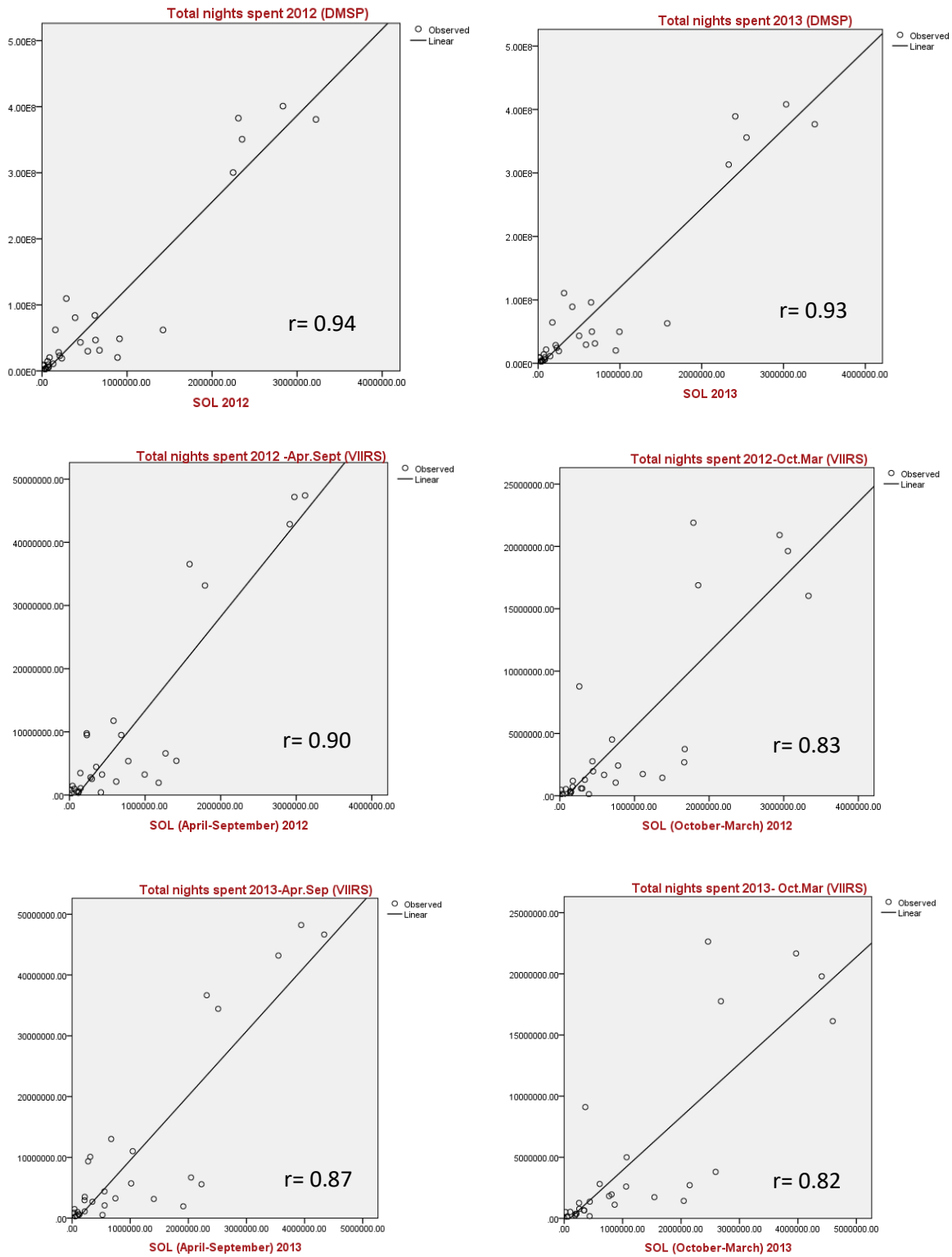


Figure 13 Linear relationship test between the studies variables

***Assumption 2: No significant outliers should be presented***

From the above scatterplots, the observed data do not have dependent variables values that have a strong difference from the predicted values. Thus, there is an absence of significant outliers, which could lead to a poor model fit.

***Assumption 3: Independence of observations is needed***

One of the assumptions of regression is that observations are not depended. In cross sectional analysis, there is no need to worry about independence assumption, because it is “assumed” to be met (Bansal, 2018).

***4.3.2 Geographically Weighted regression (GWR)***

In recent years, the Geographical Weighted Regression (GWR) method has been applied in a variety of domains in order to investigate spatial variations (Chalkias et al., 2013). The geographically weighted regression is the first alternative approach to overcome the lack of spatial stability (Fotheringham and Charlton, 1998). It is a variation of single or multiple linear regression. Its difference lies in the fact that the observations are weighted by their geographic location. This has as a direct result in the analysis: in classical regression (OLS) is becoming in supra – scale (global model), while in the geographically weighted regression in local scale (local model)(Fotheringham et al., 2012 and Milaka, 2010 and kalogirou 2003). The formula of the geographically weighted regression is as follows:

$$Y_i = \beta_{0i} + \sum_j \chi_{ij} \beta_j(\rho_i) + \varepsilon_i$$

where  $\rho_i$  is the geographic location of observation  $i$ . A fundamental idea of geographically weighted regression is the calculation of the parameters  $\beta_j(\rho_i)$  for each variable  $j$  and for each spatial unit  $i$  (summed  $\beta_{ij}$ ) (Palanga and Fotis, 2011).

The spatial autocorrelation (global Moran’s I) of the above variables is also examined, in order to identify the spatial pattern of residuals. When Moran's I gets values greater than 0, then the set of observations shows a grouped spatial pattern, while for less than 0 shows a scattered pattern. In these cases, a Geographically Weighted regression is conducted, by using the method AIC (Akaike Information Criterion) (through ArcGis software) where the system automatically calculates the optimal number of neighbours.

## 5. RESULTS

Total Nights Spent at the national level for Europe was correlated with the sum of lights, obtained by both DMSP and VIIRS night light images.

### 5.1 DMSP regression results

Starting by setting as dependent variable the ‘Total nights spent 2012’ and as independent the SOL 2012, we came across the following results (figure 14):

Model Summary <sup>b</sup>									
Model	R	R Square	Adjusted R Square	Std. Error of the Estimate	R Square Change	F Change	df1	df2	Sig. F Change
1	.943 <sup>a</sup>	.890	.886	43216720.53	.890	234.723	1	29	.000

a. Predictors: (Constant), SOL2012  
b. Dependent Variable: TotalNightsSpent2012

ANOVA <sup>a</sup>						
Model		Sum of Squares	df	Mean Square	F	Sig.
1	Regression	4.384E+17	1	4.384E+17	234.723	.000 <sup>b</sup>
	Residual	5.416E+16	29	1.868E+15		
	Total	4.926E+17	30			

a. Dependent Variable: TotalNightsSpent2012  
b. Predictors: (Constant), SOL2012

Coefficients <sup>a</sup>								
Model		Unstandardized Coefficients		Standardized Coefficients	t	Sig.	95.0% Confidence Interval for B	
		B	Std. Error	Beta			Lower Bound	Upper Bound
1	(Constant)	-5881046.871	9719543.299		-.605	.550	-25759744.9	13997651.19
	SOL2012	130.868	8.542	.943	15.321	.000	113.398	148.338

a. Dependent Variable: TotalNightsSpent2012

Figure 14 Regression analysis results for DMSP 2012

The R value represents the simple correlation and is 0.943, which indicates very high degree of correlation. The  $R^2$  indicates the percentage of variability of SOL interpreted by the model. Possible values range from 0 to 1. Values closer to 1 indicate that the model has a better predictive character. In our case, this percentage is 89%, and is very high too. Going to the ANOVA table, it is indicated by the Sig. column (where the statistical significance is indicated) that the regression model predicts the depended variable, significantly well. Here  $p=0.0000$  ( $p<0.0005$ ). The coefficients table provides the necessary information in order to predict the Total Nights Spent from the Sum of Lights (SOL), by using the values from column B. The regression equation is as follows:

$$\text{TotalNightsSpent2012} = -5881047 + 131 * \text{SOL2012}$$

The model shows that there is a positive correlation between the two variables. A schematic presentation of the linear regression model by using the Ordinary Least Squares is given in the figure 15 below:

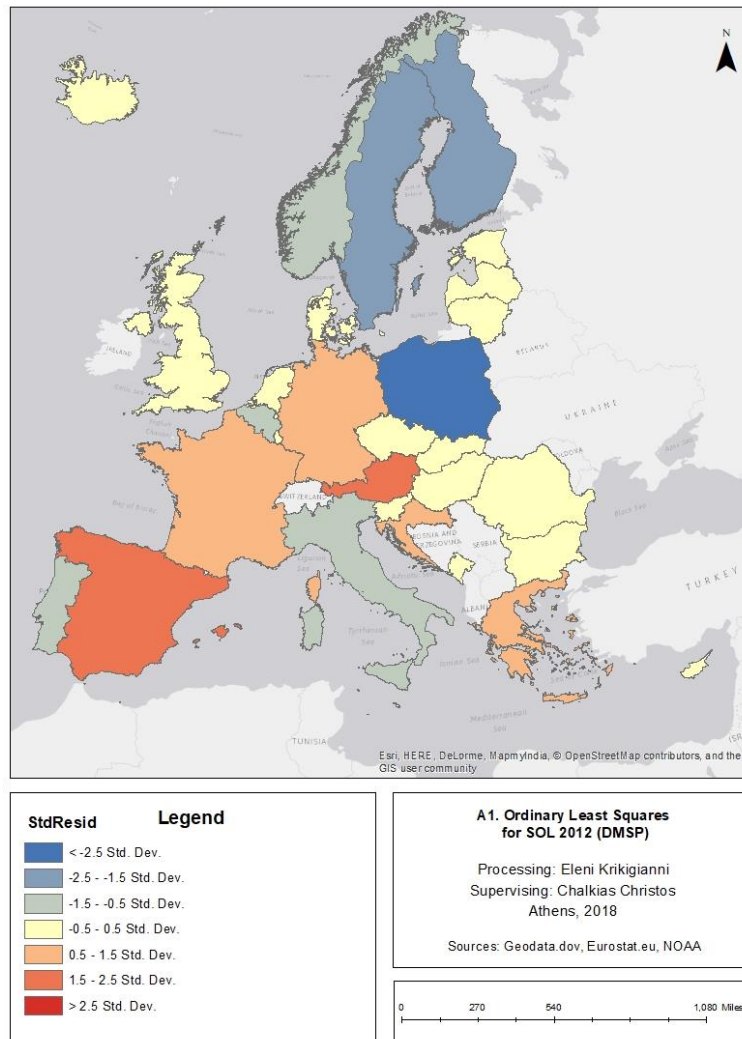


Figure 15 Ordinary Least Squares for SOL 2012-Residuals

The underestimations are presented in the areas depicted in the shades of red colour, while overestimations are presented in areas depicted in the shades of blue colour. The satisfactory performance of the model is depicted by the absence of a specific structure (eg grouping) in overestimations and in underestimations.

For further examination of the spatial relationships and exploration of potential geographical heterogeneities, Moran's I index has been calculated, in order to check if the residuals have a random pattern.

Taken this spatial autocorrelation tool, it is assumed as a null hypothesis that there is no spatial grouping for the values associated with geographic data of the study area. For a small p-value and a large absolute z-score value, the zero hypothesis is discarded. When the index gets values higher than 0, then the set of observations shows a grouped spatial pattern while for less than 0 a scattered pattern is presented. As shown by z-score (0.974469) and p-value (0.3298) the residuals' pattern doesn't appear to be significantly different than random (figure 16).

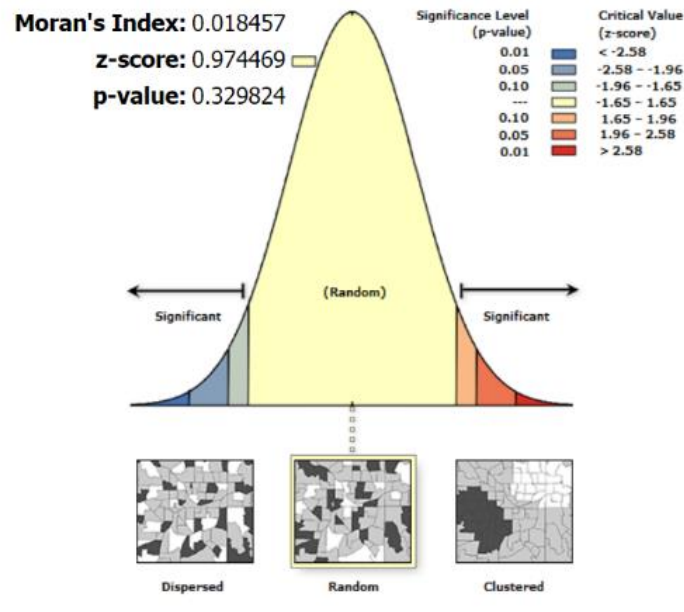


Figure 16 Spatial Autocorrelation Report for DMSP 2012

Given the residuals do not appear to follow a specific pattern (e.g. dispersed or clustered) and are independently and identically distributed around a mean of zero, a Geographically Weighted Regression is not applied in this case.

Continuing with the dependent variable 'Total nights spent 2013' and the independent variable of SOL 2013 and based on the outputs given in figures 17-19 below, the model shows that there is a positive correlation between the two variables ( $\text{TotalNightsSpent2013} = -5272233 + 125 \cdot \text{SOL2013}$ ) and there are not significant differences with the model of 2012.

At this stage, we can assume that DMSP analysis indicates positive results regarding the ability of the model to interpret the variables under investigation. In the next chapter, data will be tested on a six-month basis (deriving from monthly raw data) for the same years, to examine the level of correlation between the examined variables.

**Model Summary**

Model	R	R Square	Adjusted R Square	Std. Error of the Estimate	R Square Change	Change Statistics			Sig. F Change
						F Change	df1	df2	
1	.939 <sup>a</sup>	.881	.877	45603523.62	.881	214.360	1	29	.000

a. Predictors: (Constant), SOL2013

**ANOVA<sup>a</sup>**

Model		Sum of Squares	df	Mean Square	F	Sig.
1	Regression	4.458E+17	1	4.458E+17	214.360	.000 <sup>b</sup>
	Residual	6.031E+16	29	2.080E+15		
	Total	5.061E+17	30			

a. Dependent Variable: TotalNightsSpent2013  
b. Predictors: (Constant), SOL2013

**Coefficients<sup>a</sup>**

Model		Unstandardized Coefficients		Standardized Coefficients	t	Sig.	95.0% Confidence Interval for B	
		B	Std. Error				Lower Bound	Upper Bound
1	(Constant)	-5272233.058	10283987.19		-.513	.612	-26305348.5	15760882.39
	SOL2013	124.702	8.517	.939	14.641	.000	107.282	142.122

a. Dependent Variable: TotalNightsSpent2013

Figure 17 Regression analysis results for DMSP 2013

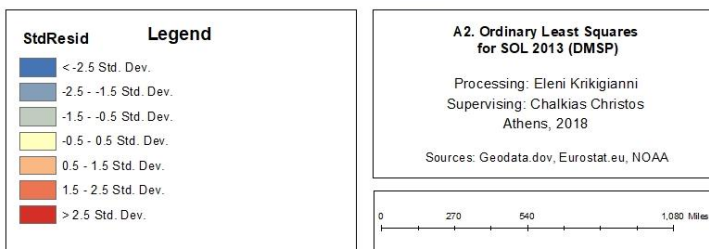
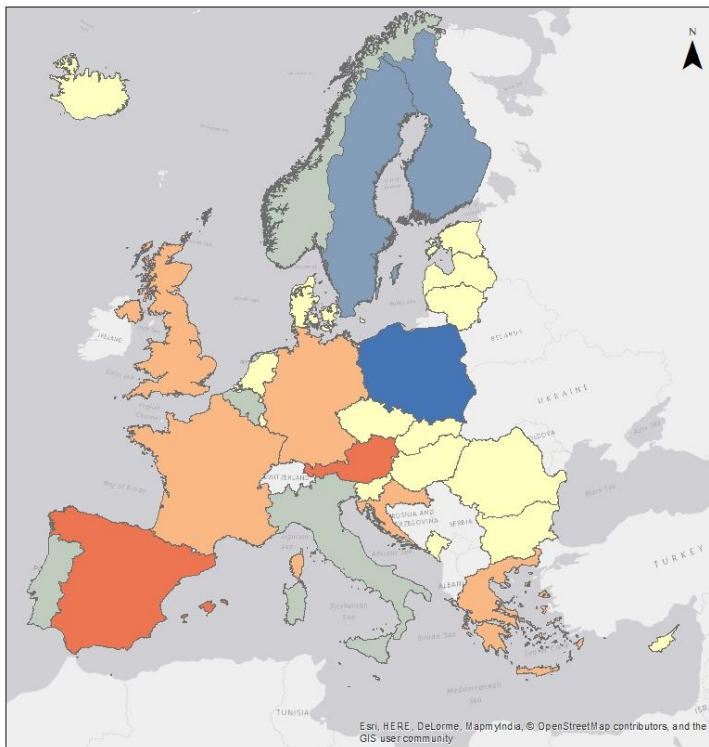


Figure 19 Ordinary Least Squares for SOL 2013-Residuals

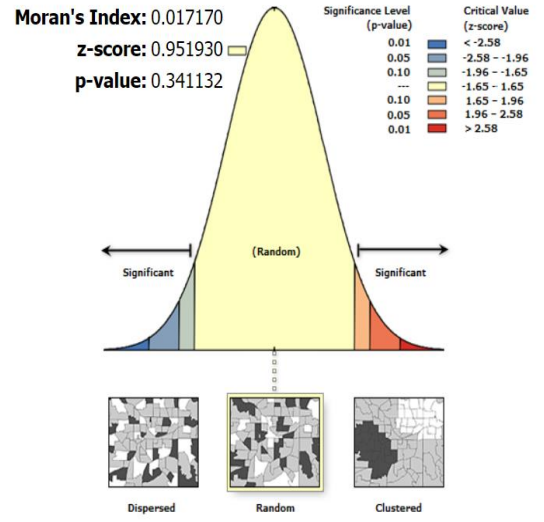


Figure 18 Spatial Autocorrelation Report for DMSP 2013

### 5.2 VIIRS regression results

By examining the variables on a semester basis (April to September and October to March) of 2012 & 2013 we came across the following results (figures 20-31):

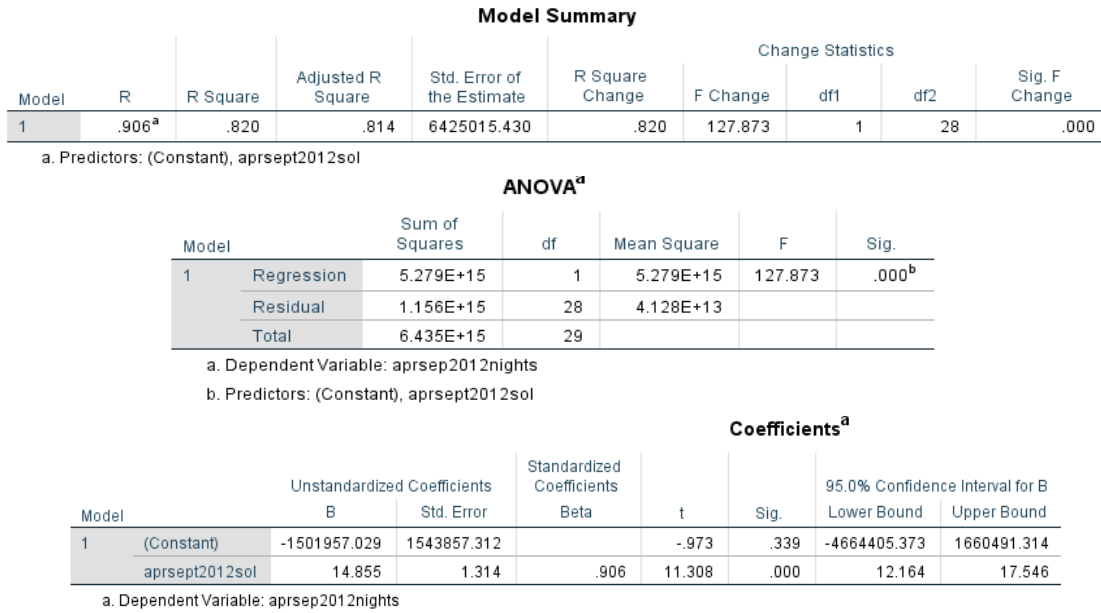


Figure 20 Regression analysis results for VIIRS Apr-Sept 2012

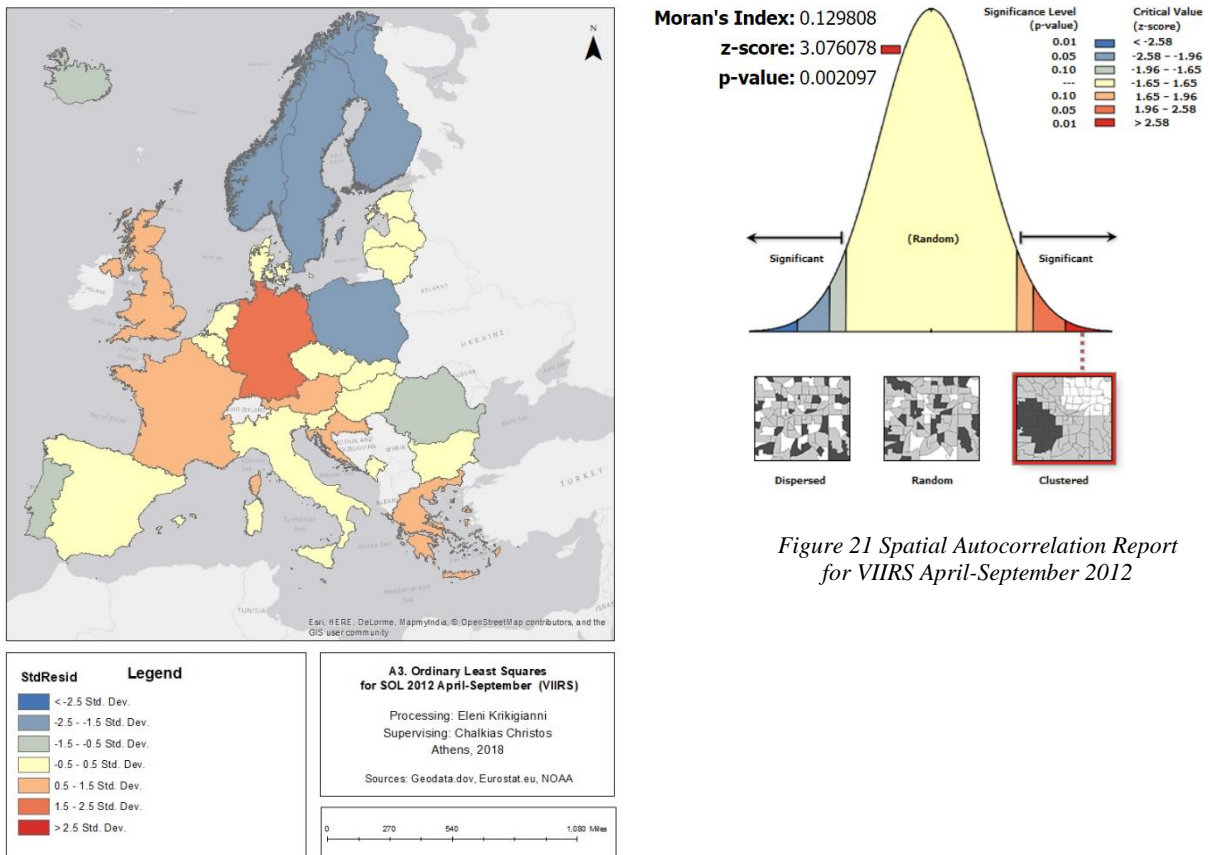


Figure 21 Spatial Autocorrelation Report for VIIRS April-September 2012

Figure 22 Ordinary Least Squares for SOL 2012 (April-Sept)

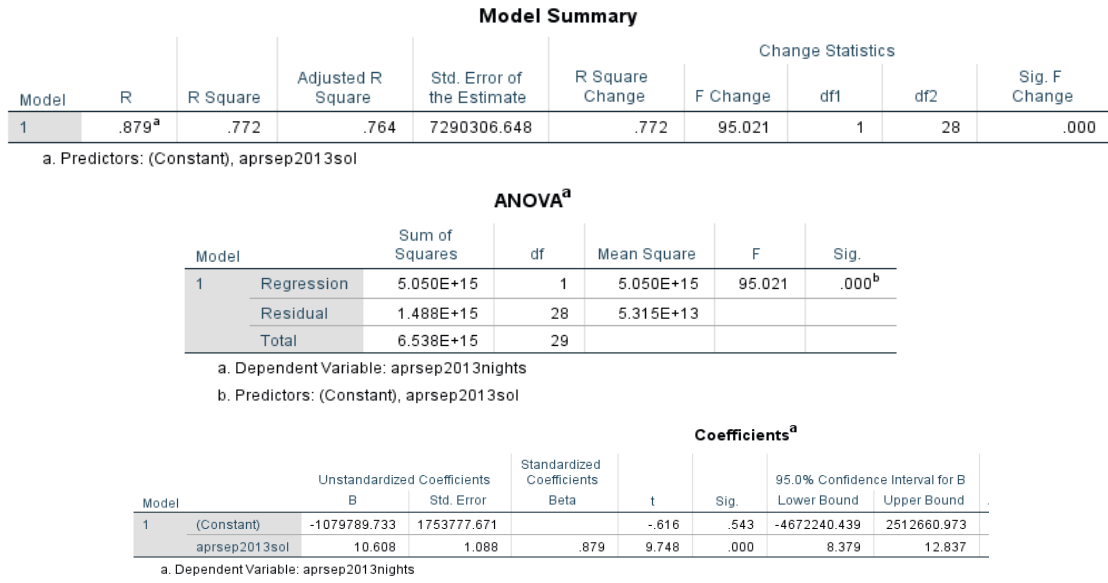


Figure 23 Regression analysis results for VIIRS Apr-Sept 2013

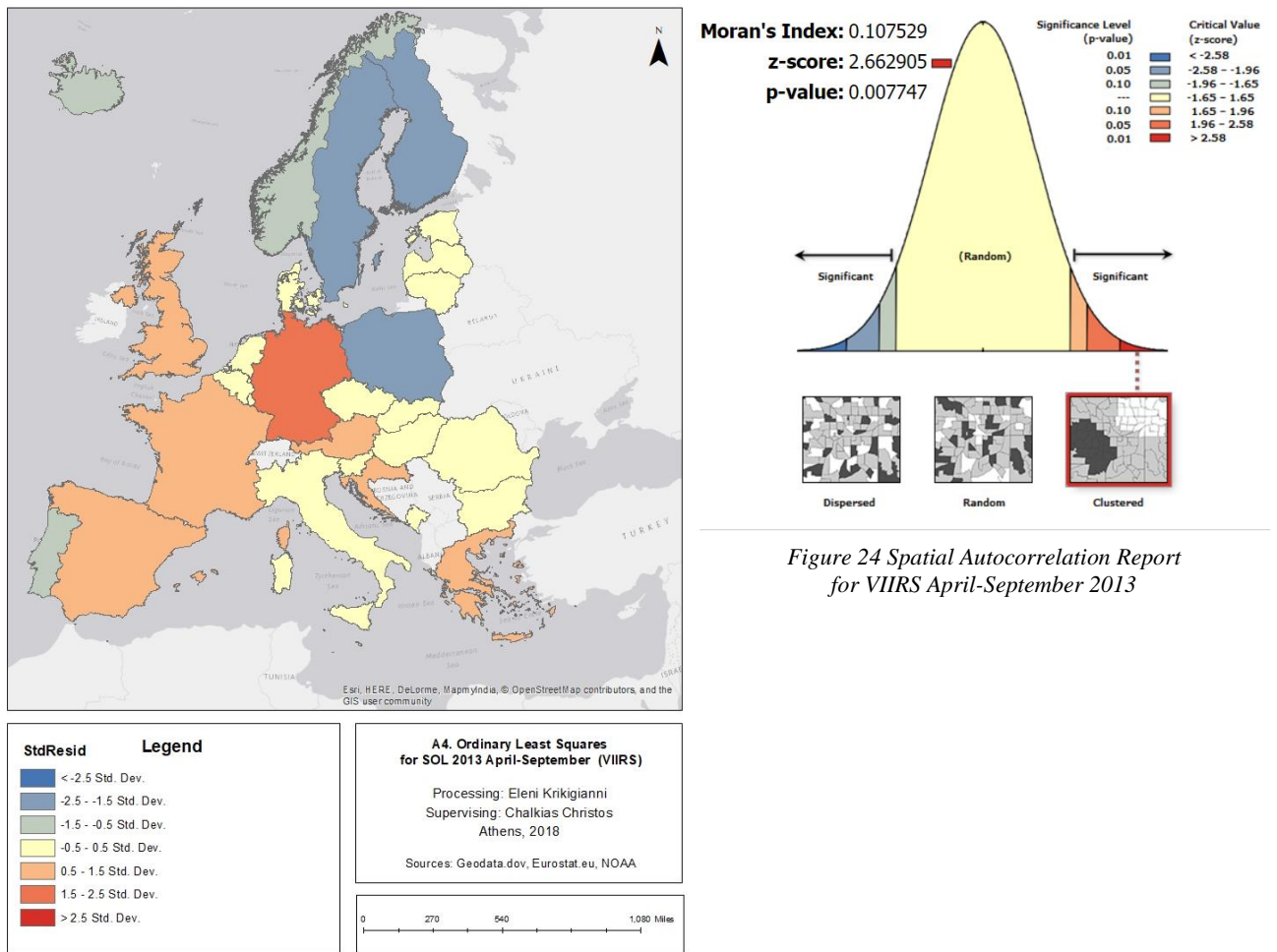


Figure 24 Spatial Autocorrelation Report for VIIRS April-September 2013

Figure 25 Ordinary Least Squares for SOL 2013 (April-Sept)

**Model Summary**

Model	R	R Square	Adjusted R Square	Std. Error of the Estimate	R Square Change	Change Statistics			Sig. F Change
						F Change	df1	df2	
1	.834 <sup>a</sup>	.695	.684	3891105.857	.695	63.739	1	28	.000

a. Predictors: (Constant), oktmar2012sol

**ANOVA<sup>a</sup>**

Model		Sum of Squares	df	Mean Square	F	Sig.
1	Regression	9.651E+14	1	9.651E+14	63.739	.000 <sup>b</sup>
	Residual	4.239E+14	28	1.514E+13		
	Total	1.389E+15	29			

a. Dependent Variable: oktmar2012nights

b. Predictors: (Constant), oktmar2012sol

**Coefficients<sup>a</sup>**

Model		Unstandardized Coefficients		Standardized Coefficients	t	Sig.	95.0% Confidence Interval for B	
		B	Std. Error				Lower Bound	Upper Bound
1	(Constant)	-527749.012	948799.553		-.556	.582	-2471276.793	1415778.769
	oktmar2012sol	6.021	.754	.834	7.984	.000	4.476	7.566

a. Dependent Variable: oktmar2012nights

Figure 26 Regression analysis results for VIIRS Oct-Mar 2012

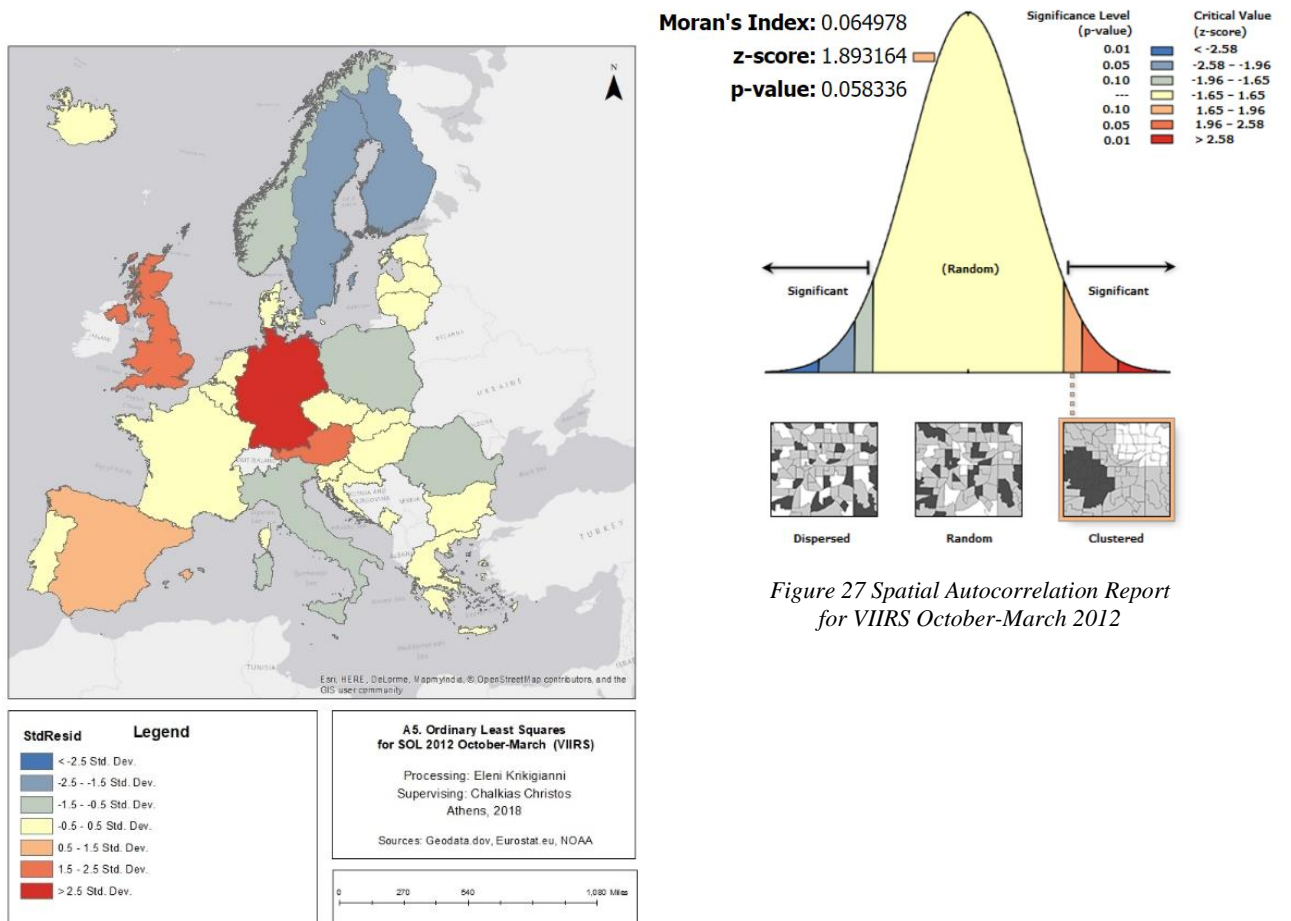


Figure 28 Ordinary Least Squares for SOL 2012 (Oct-March)

**Model Summary**

Model	R	R Square	Adjusted R Square	Std. Error of the Estimate	R Square Change	Change Statistics			Sig. F Change
						F Change	df1	df2	
1	.825 <sup>a</sup>	.681	.670	4086387.865	.681	59.833	1	28	.000

a. Predictors: (Constant), oktmar2013sol

**ANOVA<sup>a</sup>**

Model		Sum of Squares	df	Mean Square	F	Sig.
1	Regression	9.991E+14	1	9.991E+14	59.833	.000 <sup>b</sup>
	Residual	4.676E+14	28	1.670E+13		
	Total	1.467E+15	29			

a. Dependent Variable: oktmar2013nights

b. Predictors: (Constant), oktmar2013sol

**Coefficients<sup>a</sup>**

Model		Unstandardized Coefficients		Standardized Coefficients Beta	t	Sig.	95.0% Confidence Interval for B	
		B	Std. Error				Lower Bound	Upper Bound
1	(Constant)	-428688.884	993214.254		-.432	.669	-2463196.055	1605818.287
	oktmar2013sol	4.361	.564	.825	7.735	.000	3.206	5.516

a. Dependent Variable: oktmar2013nights

Figure 29 Regression analysis results for VIIRS Oct-Mar 2013

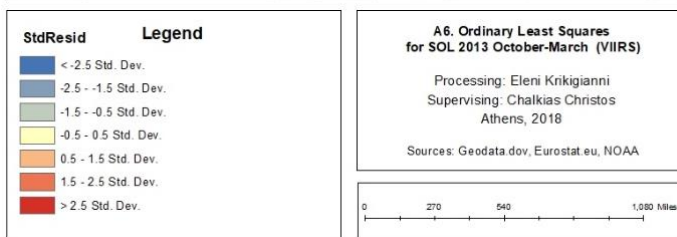
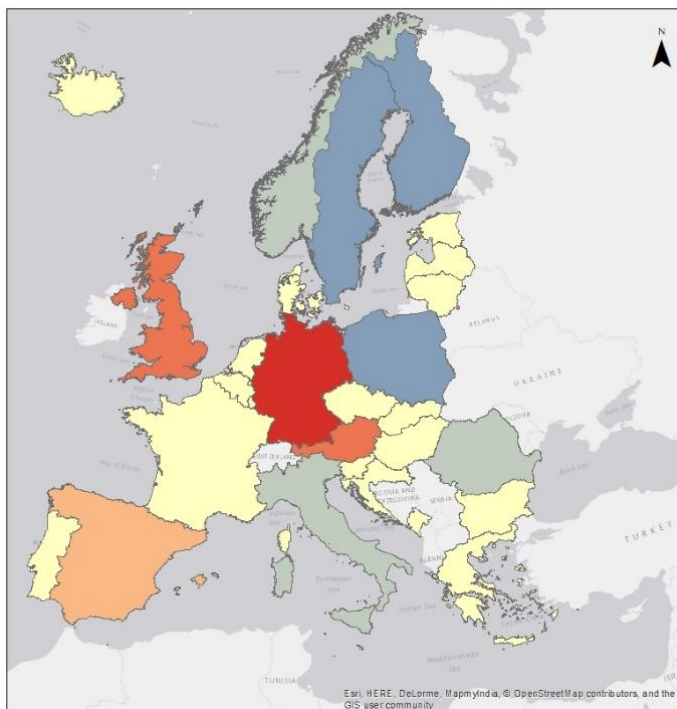


Figure 31 Ordinary Least Squares for SOL 2013 (Oct-March)

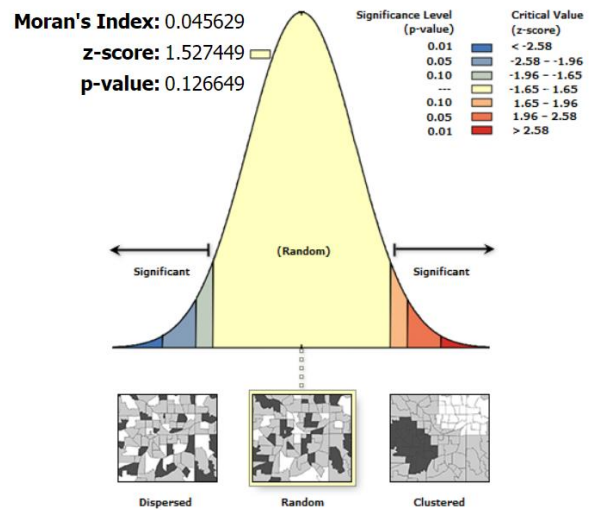


Figure 30 Spatial Autocorrelation Report for VIIRS October-March 2013

Given the z-score of 3.0761 (for Apr-Sept 2012) and 2.6629 (for Apr-Sept 2013), there is a less than 1% likelihood that this clustered pattern could be the result of random chance. Also, the z-score of 1.8931 (for Oct-Mar 2012) indicates that there is a less than 10% likelihood that this clustered pattern could be the result of random chance. However, for Oct-Mar 2013 although the given z-score of 1.5274, reflects a pattern, which does not appear to be significantly different than random, the R<sup>2</sup> (68%) indicates not quite high degree of correlation between the examined variables.

To further examine the spatial heterogeneity and the variance of the residuals, a geographically weighted regression (GWR) with adaptive spatial kernels is employed (Fotheringham et al., 2011). In this context ArcGIS GWR is used. The AIC (Akaike Information Criterion) method is used to calculate the bandwidth. With this method, the system automatically calculates the optimal number of neighbours. The input features (Dependent and Explanatory variables) are the same with those specified in the OLS models. Individual results are presented in tables 8 and 9 and cumulative ones in table 10 below:

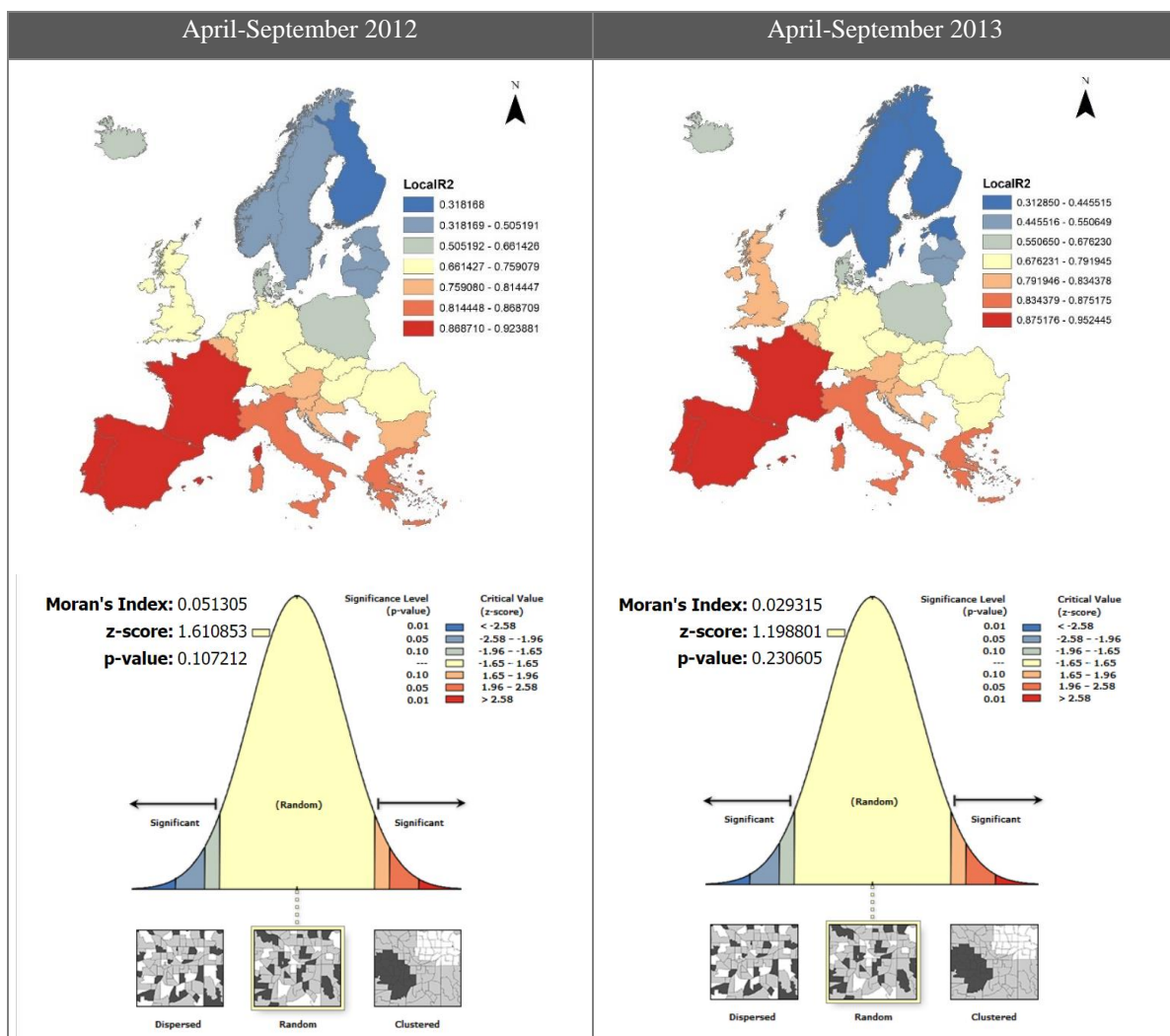


Table 8 GWR results for April-September 2012 (left) and 2013 (right)

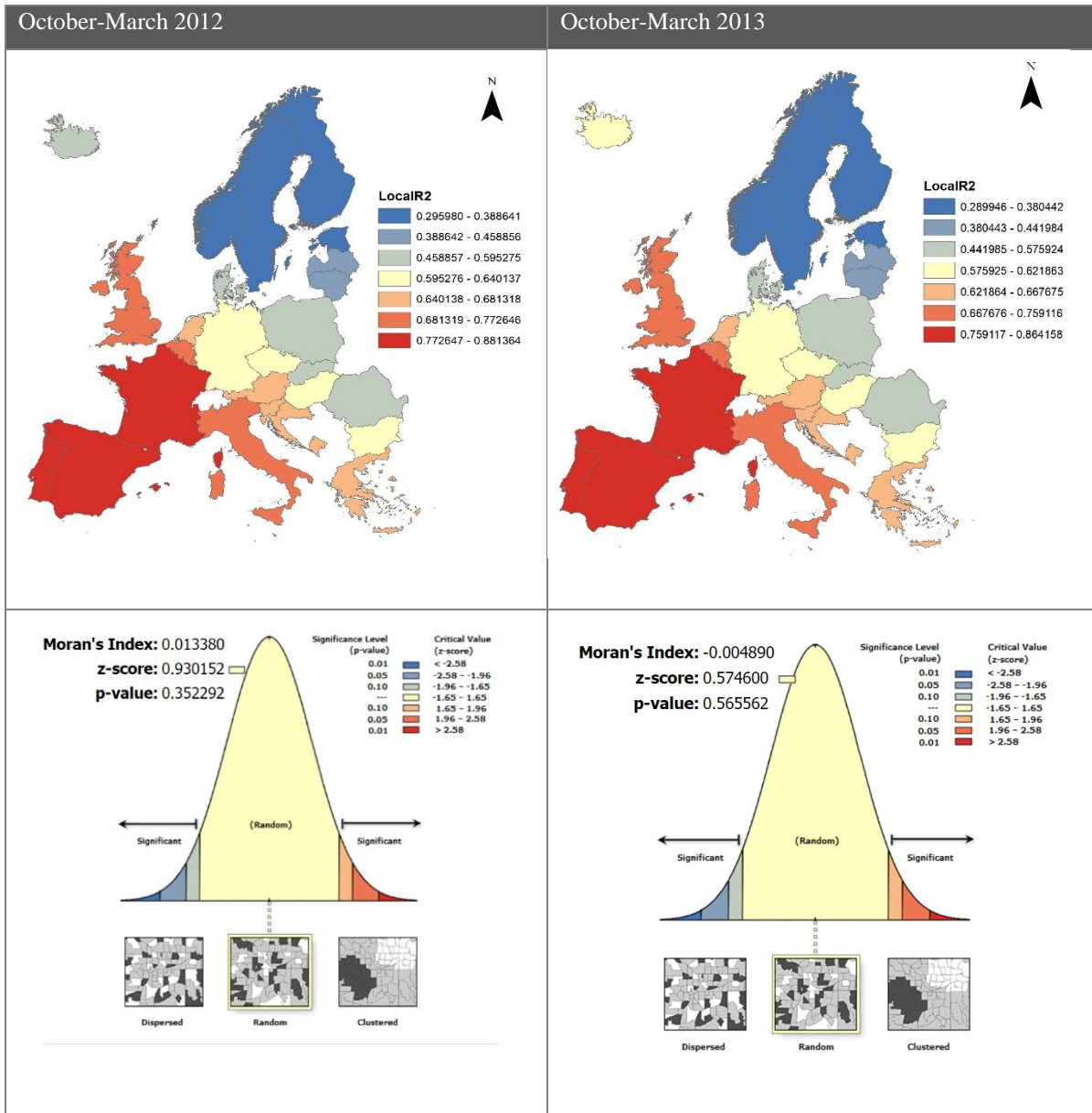


Table 9 GWR results for October-March 2012 (left) and 2013 (right)

Following the execution of GWR, higher values of the coefficient of determination  $R^2$  are depicted in the southern countries of Europe for both the summer and winter period; this indicates that the method performs better in Southern Europe rather than in Northern Europe. These values are systematically higher for the summer period analysis indicating stronger correlation during the summer period. The relatively lower values of  $R^2$  in north Europe, could be explained either form the existence of indoor activities or from other geomorphological elements (i.e. snow cover, albedo, etc.) that affect the captures of VIIRS sensor.

Indexes	Apr-Sep 2012	Apr-Sep 2013	Oct-Mar 2012	Oct-Mar 2013
<b>OLS</b>				
<b>R<sup>2</sup></b>	0.82	0.72	0.65	0.68
<b>Pearson</b>	0.90	0.87	0.83	0.87
<b>Moran's I</b>	0.129808	0.107529	0.064978	0.045629
<b>z-scope</b>	3.076078	2.662905	1.893164	1.527449
<b>p-value</b>	0.002097	0.007747	0.058336	0.126649
<b>AICc</b>	1030.53	1038.11	1000.44	1003.37
<b>GWR</b>				
<b>R<sup>2</sup></b>	0.32-0.92	0.31-0.95	0.30-0.88	0.29-0.86
<b>R<sup>2</sup>(Mean)</b>	0.72	0.74	0.62	0.61
<b>Moran's I</b>	0.051305	0.029315	0.013380	-0.004890
<b>z-scope</b>	1.610853	1.198801	0.930152	0.574600
<b>p-value</b>	0.107212	0.230605	0.352292	0.565562
<b>AICc</b>	1497.048	1023.79	997.57	1001.17

Table 10 Cumulative presentation of results from OLS and GWR regressions

The diagnostic statistics, which are derived from ArcGis and SPSS, provide a good indication of the existence of possible goodness of fit of the model (Fotheringham et al, 2011).

Any spatial dependences which were presented in the residuals for the global model, have been removed with the geographical weighting in the local model (Moran's I index). The local mean R<sup>2</sup> takes slightly higher values, and this is a good token of improvement in the model performance. Also, by comparing the global model's AICc value with the local model's AICc value, is evident that in three out of four cases, the lower values in the local model, depict a strong evidence of an improvement in the fit of the model to the data, namely a better performance for the local model. This improvement can be also statistically supported and verified by the calculated Moran's I index in the local model, which shows lower variances and higher probabilities of random distribution (p-values and z-scores).

The relationship between nights spent in a place and DMSP generated SOL is positive, suggesting areas with higher SOL have a better touristic activity, in terms of nights spent in these areas. The global model of VIIRS appears to follow this positive correlation between the examined variables. Besides, the local regression model shows that this relationship is stronger in Southern Europe during the summer, where there is a pick in touristic activity. From the

above mentioned seems that the association between Touristic activities and Night time emissions, although evident is not homogeneous in both spatial and temporal terms.

Seasonality of Touristic activity is well captured by Seasonal Night light images. This would appear to be a strong argument in favour of receiving funds, policy making and resource use and conservation. Results, also, show that the nights spent in a place have better correlation with SOL during the summer period (April-September), in comparison with the winter period (October-March), where the correlation is lower (<80%), but still in high level. This difference may have arisen either from the calculation process been followed for the data of the warmer period (April – September) either from the existence of other parameters (i.e. Indoor activities, land cover, albedo, etc) (Liang at al., 2005), that based on the literature, affect the imaging of night-time light emissions.

## 6. CONCLUDING REMARKS

In this thesis, we investigate the seasonal changes in the brightness of night-time satellite images, as well as their correlation with the touristic activity in EU countries. By using a linear regression model, DMSP examination on a yearly basis, showed a strong positive relationship between the variables under investigation. VIIRS global examination, showed that the positive relationship still exists on a semester basis, but the level of correlation is different between the winter and summer periods. The local model (GWR) in VIIRS, produced better results in terms of goodness of fit of the model and residuals independency than the global model (OLS). Also, from the local regression analysis it can be assumed that the model works better for the South Europe. It is also worth mentioning, that in future researches possible use of complete data series of light emission (without forecasted images), as well as the -simultaneous- investigation of other variables (like population and/or GDP, or energy consumption) could interpret better the relationship between the examined variables and could give better results in the assessment of the model.

Besides, considering also that the examined socioeconomic variable (total nights spent) has a strong relationship with the space, it is highly recommended a further investigation of its correlation with the SOL index, by taking into account categories of areas around Europe (geographical heterogeneity) e.g. North and South Europe, and/or examine the level of their correlation in other spatial classification (e.g. nuts 1 or nuts 2). Thus, a stratified more detailed spatially analysis could provide more reliable results.

In addition, the existence of other parameters that affect the recording of nightlight emission sources, (like albedo, land cover etc), should be also investigated, in order to determine and specify the ability and the accuracy of the nightlight imaginary in the assessment of the touristic activity.

## 7. LITERATURE

- Bansal G., (2018), *What are the four assumptions of linear regression?*, Available at: <http://blog.uwgb.edu/bansalg/statistics-data-analytics/linear-regression/what-are-the-four-assumptions-of-linear-regression/> [Last access 30/01/2018].
- Carlowicz M., (2017), *New Night Lights Maps Open Up Possible Real-Time Applications*, Available at: <https://www.nasa.gov/feature/goddard/2017/new-night-lights-maps-open-up-possible-real-time-applications> [Last access 30/01/2018].
- Chalkias, C., Petrakis, M. Psiloglou B., Lianou M., (2005): *Modelling of light pollution in suburban areas using remotely sensed imagery and GIS*, Journal of Environmental Management, vol. 79. pp. 57-63.
- Chalkias C., Papadopoulos A., Kalogeropoulos K., Tambalis K., Psarra G., Sidossis L., (2013), *Geographical heterogeneity of the relationship between childhood obesity and socio-environmental status: Empirical evidence from Athens, Greece*, Volume 37, Pages 34–43, available at: <URL: <http://www.sciencedirect.com/science/article/pii/S0143622812001087> [Last access 30/01/2018].
- Cinzano P., Falchi F., Elvidge C., (2001), *The first world atlas of the artificial night sky brightness*, Monthly Notices of the Royal Astronomical Society, 328 (3), 689-707, DOI: 10.1046/j.1365-8711.2001.04882.x.
- Cozzolino E., Lasta C., (2016), *Use of VIIRS DNB satellite images to detect jigger ships involved in the *Illex argentinus* fishery*, Volume 4, October 2016, Pages 167-178, <https://doi.org/10.1016/j.rsase.2016.09.002>.
- Croft T., (1979), *The brightness of lights of earth at night, digitally recorded by DMSP satellite*, US Geological survey, available at: <https://pubs.usgs.gov/of/1980/0167/report.pdf>, [Last access 30/01/2018].
- Darlington B. R., Hayes F. A., (2017), *Regression Analysis and Linear Models: Concepts, Applications, and Implementation (Methodology in the Social Sciences)*, The Guilford Press, ISBN 978-1-4625-2113-5.
- Doll, C.H., Muller, J.P., Elvidge, C.D., (2000), *Night-time imagery as a tool for global mapping of socioeconomic parameters and greenhouse gas emissions*, AMBIO J. Hum. Environ. 2000, 29, 157–162.
- Doll Christopher N.H., (2008), *CIESIN Thematic Guide to Night-time Light Remote Sensing and its Applications*, Center for International Earth Science Information Network (CIESIN) Columbia University Palisades, NY, USA.
- Elvidge C. D., Baugh K. E., Hobson V. H., Kihn E. A., Kroehl H. W., Davis E. R., Cocero D., (1997c), *Satellite inventory of human settlements using nocturnal radiation emissions: A contribution for the global toolchest*, Global Change Biology, 3, 387.

Elvidge, C.D., Baugh, K.E., Dietz, J.B., Bland, T., Sutton, P.C. and Kroehl, H.W., (1999), *Radiance calibration of DMSP-OLS low-light imaging data of human settlements*, *Remote Sensing of Environment*, 68 (1), pp. 77-88.

Elvidge, C.D., Imhoff, M.L., Baugh, K.E., Hobson, V.R., Nelson, I., Safran, J., Dietz, J.B. and Tuttle, B.T., (2001), *Night-time lights of the world: 1994-1995*, *ISPRS Journal of Photogrammetry and Remote Sensing*, 56 (2), pp. 81-99.

Elvidge C. D., P. Cinzano, D. R. Pettit, J. Arvesen , P. Sutton , C. Small , R. Nemani , T. Longcore , C. Rich , J. Safran , J. Weeks & S. Ebener, (2007), *The Nightsat mission concept*, *International Journal of Remote Sensing*, 28:12, 2645-2670, DOI: 10.1080/01431160600981525.

Elvidge, C.D., Ziskin, D., Baugh, K.E., Tuttle, B.T., Ghosh, T., Pack, D.W., Erwin, E.H., Zhizhin, M., (2009), *A fifteen-year record of global natural gas flaring derived from satellite data*, *Energies* 2009, 2, 595–622.

Elvidge C., Baugh K., Sutton P., Bhaduri B., Tuttle B., Tilottama G., Ziskin D., Erwin E., (2010), *Who's in the Dark: Satellite Based Estimates of Electrification Rates*, Earth Observation Group, NOAA National Geophysical Data Center, 102-123.

Elvidge C., David M. Keith, Benjamin T. Tuttle, Kimberly E. Baugh, (2010), *Spectral Identification of Lighting Type and Character*, *Sensors* 2010, 10(4), 3961-3988; doi:10.3390/s100403961.

Elvidge C., Zhizhin M., Hsu F., Baugh K., (2013), *VIIRS Nightfire: Satellite Pyrometry at Night*, *Remote Sens.* 2013, 5(9), 4423-4449; doi:10.3390/rs5094423.

Elvidge, C.D., Hsu, F.-C., Baugh, K.E. and Ghosh, T., (2014), *National trends in satellite-observed lighting 1992-2012*. In Weng, Q. (ed.) *Global urban monitoring and assessment through earth observation*. Boca Raton: CRC Press, pp.96-120.

Elvidge C., Zhizhin M., Baugh K., Hsu F., (2015), *Automatic Boat Identification System for VIIRS Low Light Imaging Data*, *Remote Sensing*, DOI: 10.3390/rs70303020.

Elvidge C., Zhizhin M., Baugh K., Hsu F., Ghosh T., (2015), *Methods for Global Survey of Natural Gas Flaring from Visible Infrared Imaging Radiometer Suite Data*, *Energies* 9(1):14, DOI:10.3390/en9010014.

European Commission (EC), (2001), *Tourism Trends in Mediterranean Countries*, Available at: <http://ec.europa.eu/eurostat/documents/3217494/5628504/KS-40-01-666-FR.PDF/ff0abde3-19a9-4ea5-b7bf-11fa860a3289?version=1.0> [Last access 30/01/2018].

European Commission (EC), (2006), *Communication from the Commission: A renewed EU Tourism Policy: Towards a stronger partnership for European Tourism*, Available at: <http://eur-lex.europa.eu/legal-content/EN/TXT/PDF/?uri=CELEX:52006DC0134&from=EN> [Last access 30/01/2018].

European Commission (EC), (2018), *Tourism*, Available at: [https://ec.europa.eu/growth/sectors/tourism\\_en](https://ec.europa.eu/growth/sectors/tourism_en) [Last access 30/01/2018].

European Commission (EC), (2018), *Virtual Tourism Observatory*, Available at: <https://ec.europa.eu/growth/tools-databases/vto/> [Last access 30/01/2018].

Eurostat, (2013), *Regions in the European Union - Nomenclature of territorial units for statistics - NUTS 2013/EU-28*, Available at: <http://ec.europa.eu/eurostat/documents/3859598/6948381/KS-GQ-14-006-EN-N.pdf/b9ba3339-b121-4775-9991-d88e807628e3> [Last access 30/01/2018].

Eurostat, (2013), *The EU in the world 2013 — A statistical portrait*, Available at: <http://ec.europa.eu/eurostat/documents/3217494/5748537/KS-30-12-861-EN.PDF/d60278b9-d0ee-47c1-bb96-2dbb9a5b80cb?version=1.0> [Last access 30/01/2018].

Eurostat, (2017), *Tourism statistics*, Available at: [http://ec.europa.eu/eurostat/statistics-explained/index.php/Tourism\\_statistics#Data\\_sources\\_and\\_availability](http://ec.europa.eu/eurostat/statistics-explained/index.php/Tourism_statistics#Data_sources_and_availability) [Last access 30/01/2018].

Eurostat, (2018), *Data (Total nights spent)*, Available at: <http://ec.europa.eu/eurostat/tgm/table.do?tab=table&init=1&language=en&pcode=tin00171&plugin=1> [Last access 30/01/2018].

Fotheringham, A., Charlton, M., (1998), *Geographically weighted regression: a natural evolution of the expansion method for spatial data analysis*, Environment and Planning A, pages 1905-1927, available at: <URL: <http://epn.sagepub.com/content/30/11/1905.abstract?id=a301905> [Last access 30/01/2018].

Fotheringham, A. S., Brunsdon, C., & Charlton, M. (2002). *Geographically weighted regression: The analysis of spatially varying relationships*. Chichester: John Wiley and Sons.

Fotheringham, A., Charlton, M., (2011), *Geographically weighted regression: a tutorial on using GWR in ArcGIS 9.3*, available at: <URL: [https://www.geos.ed.ac.uk/~gisteac/fspat/gwr/gwr\\_arcgis/GWR\\_Tutorial.pdf](https://www.geos.ed.ac.uk/~gisteac/fspat/gwr/gwr_arcgis/GWR_Tutorial.pdf) [Last access 30/01/2018].

Galimberti J. K., (2017), *Forecasting GDP growth from the outer space*, available at: <https://www.research-collection.ethz.ch/handle/20.500.11850/128755> [Last access 30/01/2018].

Ghosh T., Powell R., Elvidge C., Baugh K., Sutton P., Anderson S., (2010), *Shedding Light on the Global Distribution of Economic Activity*, The Open Geography Journal, 2010, 3, 148-161, DOI: 10.2174/1874923201003010147.

Hanwei L., Liang D., Hiroki T., Xiao L., (2016), *Feasibility of a new-generation night-time light data for estimating in-use steel stock of buildings and civil engineering infrastructures*, Resources Conservation and Recycling, DOI:10.1016/j.resconrec.2016.04.001.

Hattori, R., Horie, S., Hsu, F.-C., Elvidge, C.D., Matsuno, Y., (2013), *Estimation of in-use steel stock for civil engineering and building using night-time light images*, Resour. Conserv. Recycl., <http://dx.doi.org/10.1016/j.resconrec.2013.11.007>.

- Hsu, F.-C., Daigo, I., Matsuno, Y., Adachi, Y., (2011), *Estimation of steel stock inbuilding and civil construction by satellite images*. ISIJ Int. 51, 313–319.
- Hsu, F.-C., Elvidge, C.D., Matsuno, Y., (2013), *Exploring and estimating in-use steelstocks in civil engineering and buildings from night-time lights*, Int. J. RemoteSens. 34, 490–504.
- Huang Q., Yang X., Gao B., Yang Y., Zhao Y., (2014), ‘*Application of DMSP/OLS Night-time Light Images: A Meta-Analysis and a Systematic Literature Review*, Remote Sens. 2014, 6(8), 6844-6866; doi:10.3390/rs6086844.
- Imhoff M., Lawrence W., Stutzer D., Elvidge C., (1997), *A Technique for using composite DMSP-OLS "City Lights" satellite data to map urban area*, Remote Sensing of Environment, 61, 361-370.
- Jing X., Shao X., Cao C., Fu X. and Yan L., (2016), *Comparison between the Suomi-NPP Day-Night Band and DMSP-OLS for Correlating Socio-Economic Variables at the Provincial Level in China*, Remote Sens. 2016, 8, 17; doi:10.3390/rs8010017.
- Kaifang S., Bailang Y., Yixiu H., Yingjie H., Bing Y., Zuoqi C., Liujia C., Jianping W., (2014), *Evaluating the Ability of NPP-VIIRS Night-time Light Data to Estimate the Gross Domestic Product and the Electric Power Consumption of China at Multiple Scales: A Comparison with DMSP-OLS Data*, Remote Sensing 2014, 6(2), 1705-1724; doi:10.3390/rs6021705.
- Kalogirou S., (2003), *The statistical analysis and modelling of interval migration flows within England and Wales* (Doctoral dissertation), Newcastle University Library (201 29808 1), available at: [gisc.gr/?mdocs-file=1245](http://gisc.gr/?mdocs-file=1245) [Last access 30/01/2018].
- Kathimerini, (2012), *Earth's impressive photo from NASA*, Available at: <http://www.pressreader.com/greece/kathimerini-greek/20121207/281479273721517> [Last access 30/01/2018].
- Kloog I., Haim A., Stevens R., Portnov B., (2009), *Global co-distribution of light at night (LAN) and cancers of prostate, colon, and lung in men*, Chronobiology International, 26 (1), 108-125, doi: 10.1080/07420520802694020.
- Letu H., Hara M., Tana G., Nishio F., (2010), *A saturated light correction method for DMSP/OLS night-time satellite imagery*, IEEE Trans. Geosci. Remote Sens., 50, 389–396.
- Li Xi, Huimin Xu, Xiaoling Chen and Chang Li, (2013), *Potential of NPP-VIIRS Night-time Light Imagery for Modeling the Regional Economy of China*, Remote Sensing, 2013, 5, 3057-3081; doi:10.3390/rs5063057.
- Liang S., Yu Y., Defelice T. P., (2005), *VIIRS narrowband to broadband land surface albedo conversion: formula and validation*, International Journal of Remote Sensing, Volume 26, Issue 5, 1019-1025, <https://doi.org/10.1080/01431160512331340156>.
- Lu, D., Tian, H., Zhou, G., Ge, H., (2008), *Regional mapping of human settlements in southeastern China with multisensor remotely sensed data*, Remote Sens. Environ, 112, 3668–3679.

Meng, L., Graus, W., Worrell, E., Huang, B., (2014), *Estimating CO<sub>2</sub> (carbon dioxide) emissions at urban scales by DMSP/OLS (Defense Meteorological Satellite Program's Operational Linescan System) night-time light imagery: Methodological challenges and a case study for China*. *Energy* 2014, 71, 468–478.

Milaka, K.G., (2010), *Spatial analysis of urban area's development through multivariable alternative scenario processing*, (Doctoral dissertation), Department of Planning and Regional Development, University of Thessaly, available at: <http://thesis.ekt.gr/thesisBookReader/id/19722#page/14/mode/2up> [Last access 30/01/2018].

Mukim M., Garrett K., (2013), *Tracking light from space: Innovative ways to measure economic development*, Available at: <http://blogs.worldbank.org/sustainablecities/tracking-light-space-innovative-ways-measure-economic-development> [Last access 30/01/2018].

Murak J., (2013), *Regression Analysis Using GIS*, available at: [https://libraries.mit.edu/files/gis/regression\\_presentation\\_iap2013.pdf](https://libraries.mit.edu/files/gis/regression_presentation_iap2013.pdf) [Last access 30/01/2018].

National Aeronautics and Space Administration -NASA, (2014), *Suomi National Polar-orbiting Partnership (Suomi NPP)*, Available at: <https://www.nasa.gov/directorates/heo/scan/services/missions/earth/SuomiNPP.html> [Last access 30/01/2018].

National Aeronautics and Space Administration NASA, (2018), *Joint Polar Satellite System*, Available at: <https://jointmission.gsfc.nasa.gov/viirs.html> and <https://viirsland.gsfc.nasa.gov/index.html> [Last access 30/01/2018].

National Oceanic and Atmospheric Administration-NOAA (*DMSP*), available at: <https://ngdc.noaa.gov/eog/dmsp/downloadV4composites.html> [Last access 30/01/2018].

National Oceanic and Atmospheric Administration-NOAA (*VIIRS*), available at: [https://ngdc.noaa.gov/eog/viirs/download\\_dnb\\_composites.html](https://ngdc.noaa.gov/eog/viirs/download_dnb_composites.html) [Last access 30/01/2018].

National Oceanic and Atmospheric Administration -NOAA, (2013), *Technical Report NESDIS 142, Visible Infrared Imaging Radiometer Suite (VIIRS) Sensor Data Record (SDR) User's Guide Version 1.2*, available at: [https://www.star.nesdis.noaa.gov/smcd/spb/nsun/snpp/VIIRS/VIIRS\\_SDR\\_Users\\_guide.pdf](https://www.star.nesdis.noaa.gov/smcd/spb/nsun/snpp/VIIRS/VIIRS_SDR_Users_guide.pdf) [Last access 30/01/2018].

OSCAR, (2018), *Satellite: DMSP-F18*, available at: <https://www.wmo-sat.info/oscar/satellites/view/65> [Last access 30/01/2018].

Ou J., Xiaoping L., Xia L., Meifang L., Wenkai L., (2015), *Evaluation of NPP-VIIRS Night-time Light Data for Mapping Global Fossil Fuel Combustion CO<sub>2</sub> Emissions: A Comparison with DMSP-OLS Night-time Light Data*, doi: 10.1371/journal.pone.0138310.

Palaga G., Photis G., (2011), *Methodological framework of spatial analysis of disposable income of the regions of the European Union*, available at: [http://www.prd.uth.gr/sites/spatial\\_analysis/chorika%20oidata/2003/palagga\\_photis\\_2011.pdf](http://www.prd.uth.gr/sites/spatial_analysis/chorika%20oidata/2003/palagga_photis_2011.pdf) [Last access 30/01/2018].

Raupach, M.R., Rayner, P.J., Paget, M., (2010), *Regional Variations in Spatial Structure of Nightlights, Population Density and Fossil-fuel CO<sub>2</sub> Emissions*, *Energy Policy* 2010, 38, 4756–4764.

Rayner J., Raupach M.R., Paget M., Peylin P., Koffi E., (2010), *A new global gridded data set of CO<sub>2</sub> emissions from fossil fuel combustion: Methodology and evaluation*, *Journal of Geophysical Research: Atmospheres* (1984–2012), 115(D19).

Saitoh S., Fukaya A., Saitoh K., Fumihito T., (2010), *Estimation of number of pacific saury fishing vessels using night-time visible images*, *International Archives of the Photogrammetry, Remote Sensing and Spatial Information Science*, Volume XXXVIII, Part 8, Kyoto Japan 20101013.

Scott C. 2015, *VIIRS Applications*, available at: [http://www.jpss.noaa.gov/assets/pdfs/events\\_conferences/satellite\\_conferences/2015/2.3b\\_NSC2015\\_Session\\_Scott.pdf](http://www.jpss.noaa.gov/assets/pdfs/events_conferences/satellite_conferences/2015/2.3b_NSC2015_Session_Scott.pdf) [Last access 30/01/2018].

Shi K., Huang C., Yu B., Yin B., Huang Y., Wu J., (2014a), *Evaluation of NPP-VIIRS night-time light composite data for extracting built-up urban areas*, *Remote Sens. Lett.* 5, 358–366.

Shi K., Yu B., Huang Y., Hu Y., Yin B., Chen Z., Chen L., Wu J., (2014a), *Evaluating the Ability of NPP-VIIRS Night-time Light Data to Estimate the Gross Domestic Product and the Electric Power Consumption of China at Multiple Scales: A Comparison with DMSP-OLS Data*, *Remote Sensing*, 6, pp. 1705-1724.

Shi, K., Chen, Y., Yu, B., Xu, T., Chen, Z., Liu, R., Li, L., Wu, J., (2016), *Modelling spatiotemporal CO<sub>2</sub> (carbon dioxide) emission dynamics in China from DMSP-OLS night-time stable light data using panel data analysis*, *Appl. Energy* 2016, 168, 528–533.

Small, C., Pozzi, F., Elvidge, C.D., (2005), *Spatial analysis of global urban extent from DMSP-OLS night lights*, *Remote Sens. Environ.*, 96, 277–291.

Stathakis D., (2016), *Forecasting urban expansion based on night lights*, *The International Archives of the Photogrammetry, Remote Sensing and Spatial Information Sciences*, Volume XLI-B8, XXIII ISPRS Congress, 12–19 July 2016, Prague, Czech Republic.

Stevenson N., Aiery D., Miller G., (2008), *Tourism policy making: the policymakers' perspectives*, available at: <http://epubs.surrey.ac.uk/1118/1/fulltext.pdf> [Last access 30/01/2018].

Su, Y., Chen, X., Li, Y., Liao, J., Ye, Y., Zhang, H., Huang, N., Kuang, Y., (2014), *China's 19-Year City-Level Carbon Emissions of Energy Consumptions, Driving Forces and Regionalized Mitigation Guidelines*, *Renew Sustain Energy, Rev.* 2014, 35, 231–243.

Sutton P., (1997), *Modelling population density with night-time satellite imagery and GIS*, *Computers, Environment and Urban Systems*, Volume 21, Issues 3–4, May–July 1997, Pages 227-244.

Sutton P., Roberts D., Elvidge C., Baugh K., (2001), *Census from Heaven: An estimate of the global human population using night-time satellite imagery*, International Journal of Remote Sensing, 22 (16), 3061-3076.

UNWTO, (2017), *Tourism Highlights: 2017 Edition*, ISBN: 978-92-844-1901-2, available at: <https://www.e-unwto.org/doi/book/10.18111/9789284419029> [Last access 30/01/2018].

Wei Y., Hongxing L. Wei S., Bailang Y., Chunliang X., (2014), *Normalization of time series DMSP-OLS night-time light images for urban growth analysis with Pseudo Invariant Features*, Volume 128, August 2014, Pages 1-13, <https://doi.org/10.1016/j.landurbplan.2014.04.015>.

Wood E., (2017), *Developing Consistent Earth System Data Records for the Global Terrestrial Water Cycle*, available at: <https://earthdata.nasa.gov/community/community-data-system-programs/measures-projects/developing-consistent-esdr-for-the-gtwc> [Last access 30/01/2018].

Xin J., Xi S., Changyong C. Xiaodong F., Lei Y., (2015), *Comparison between the Suomi-NPP Day-Night Band and DMSP-OLS for Correlating Socio-Economic Variables at the Provincial Level in China*, Remote Sens. 2016, 8(1), 17; doi:10.3390/rs8010017.

Zhang Q., Seto K., (2011), *Mapping urbanization dynamics at regional and global scales using multi-temporal DMSP/OLS night-time light data*, Volume 115, Issue 9, 15 September 2011, Pages 2320-2329, <https://doi.org/10.1016/j.rse.2011.04.032>.

Zhang X., Wu J., Peng J., Cao Q., (2017), *The Uncertainty of Night-time Light Data in Estimating Carbon Dioxide Emissions in China: A Comparison between DMSP-OLS and NPP-VIIRS*, Remote Sens. 2017, 9(8), 797; doi:10.3390/rs9080797.

Zhao N., Hsu F., Cao G., and Samson E., (2017), *Improving accuracy of economic estimations with VIIRS DNB image products*, International Journal of Remote Sensing, DOI: 10.1080/01431161.2017.1331060.

## 8. APPENDIXES

## Appendix I: Sum of Lights (SOL) for VIIRS 2012 monthly composites

NUTS_ID	Jan-12	Feb-12	Mar-12	Apr-12	May-12	Jun-12	Jul-12	Aug-12	Sep-12	Oct-12	Nov-12	Dec-12
AT	216946	235982	215842	240465	214415	246264	212841	254717	210531	263393	224109	405364
BE	224872	302065	267207	367053	321964	451114	394918	565400	487112	699950	531301	644560
BG	274145	299338	268953	301540	262238	304388	253606	306646	242439	313642	256997	391578
CZ	267488	300523	285128	327858	307945	363214	336068	408797	373789	467104	404840	894536
DE	1208091	1350990	1286593	1471429	1388132	1627213	1522327	1835182	1692701	2089551	1823488	2977755
DK	119556	140691	121326	148663	123614	158975	127713	171669	131852	191301	141416	330604
ES	2020338	2271013	2228577	2552818	2497928	2917325	2840230	3380244	3296947	4029827	3610584	3506054
EL	450039	489334	480447	531274	519779	585523	568871	654830	633619	749087	691016	699948
EE	101098	119343	95785	119383	88912	119436	80376	120457	68928	120269	71751	319764
FR	2095765	2391563	2287123	2669729	2534640	3029530	2854726	3497174	3270692	4111077	3562311	3890833
FI	1134345	910900	1206735	917715	1300369	926530	1419383	937292	1575113	953692	1708482	2322252
IS	403486	268361	442656	267876	493321	267248	556722	266850	640933	267354	701563	255298
IT	1888947	2094832	2211329	2477636	2628322	2972783	3160249	3602213	3859539	4451616	4232917	5110400
HU	254910	291595	257949	305399	261879	323255	267565	345270	274278	374770	291658	533787
HR	173122	207953	180256	225309	189483	247758	203595	279951	220124	319990	237724	585297
NO	1020266	802066	1070434	788199	1135325	770262	1213080	740665	1319296	721427	1435866	1617974
ME	36014	40498	35874	41675	35694	43197	36168	46060	36275	49127	38415	63298
MT	7234	8968	9114	11357	11545	14446	14339	18087	18313	24316	20937	23970
NL	359316	443548	435928	544879	535023	675948	668182	849402	835183	1062029	903645	991210
LU	13796	18839	15843	22365	18491	26927	21976	33024	26536	40748	29184	33569
LI	640	727	704	817	788	933	1013	1271	1182	1290	1129	2588
LT	136460	159676	126429	156459	113454	152297	96856	147120	75254	139735	76723	269432
LV	134837	152913	124562	147944	111273	141516	95195	133437	73249	122442	73979	244157
PL	988648	1128428	1038077	1218879	1102013	1335875	1187568	1487842	1295004	1685403	1394016	3808784
SE	1384963	1194116	1444519	1197664	1521552	1202252	1617453	1203404	1745096	1216320	1887296	2874520
RO	587482	669023	575960	681430	561055	697478	539370	716687	513906	744998	548325	1360672
PT	505102	502232	584775	581063	687831	683028	854315	841789	1019422	1016252	1113290	957234
SK	130392	149302	130829	155288	131395	163032	131862	172771	132766	185580	141898	295422
SI	55855	65525	56600	69109	57563	73743	58471	79629	59851	86483	63185	161873
UK	1200744	1265953	1364371	1448717	1576017	1685116	1849759	1989272	2204947	2398940	2417843	2474808

## Appendix II: Sum of Lights (SOL) for VIIRS 2013 monthly composites

NUTS_ID	Jan-13	Feb-13	Mar-13	Apr-13	May-13	Jun-13	Jul-13	Aug-13	Sep-13	Oct-13	Nov-13	Dec-13
AT	433749	440306	324250	375798	368993	223883	223883	223883	234011	301205	382183	289328
BE	1078001	784105	965073	786346	711071	745154	745154	745154	737820	751339	672911	618421
BG	417659	267714	319217	182609	176075	227520	227520	227520	237514	341986	387812	297788
CZ	800863	740217	547203	724762	697002	476404	476404	476404	487351	533702	536689	484694
DE	2713894	3052688	2819759	2908097	2821635	2001306	2064445	2001306	2101993	2260355	2123215	1802473
DK	364529	310849	243061	283264	302646	157112	201770	157112	201770	200125	211076	198592
ES	3655284	3888671	3775648	3501063	3198816	3645289	3645289	3645289	3664385	4139140	4326870	4031045
EL	699831	677918	785388	587584	546007	719651	719651	719651	741884	845506	824722	782065
EE	335545	231904	293024	184144	196207	76588	109869	76588	109869	127266	148113	132422
FR	4761352	4644068	4533153	4282792	3982540	3831068	3831068	3831068	3890361	4286412	4160491	4057025
FI	2885071	2408731	1867514	2208883	2340418	1462170	1999649	1462170	1999649	1735787	1648042	1734315
IS	464008	655006	3950	644162	674015	421640	487624	421640	487624	379795	749591	364741
IT	4327734	5207609	4268779	5067536	4621931	4078636	4078636	4078636	4100223	4227084	4787108	4757014
HU	532495	455636	455463	387362	381506	328711	328711	328711	342014	419716	405668	363290
HR	298810	417028	359666	379986	355595	282404	282404	282404	293161	326544	342633	315377
NO	1984724	2374236	818376	2065350	2208381	878131	1202671	878131	1202671	1093218	1554670	1434918
ME	54423	58022	49368	47062	43927	38776	38776	38776	39903	52383	50163	49260
MT	20715	23138	24044	21854	19406	23524	23524	23524	22990	24985	25490	25367
NL	1202834	1134010	969742	1133944	1047332	1012801	1029827	1012801	1018562	1022501	1077670	1006124
LU	65122	72965	58534	72758	65549	46470	46470	46470	46514	47197	35029	31212
LI	1684	2324	1551	2248	2103	853	853	853	879	936	1708	1633
LT	304671	215845	222800	137669	148207	75063	108994	75063	108994	145986	155782	124467
LV	321519	191016	204058	112660	120713	61623	81882	61623	81882	131116	149046	132327
PL	3849191	2750387	3160383	2607893	2534816	1722614	1837186	1722614	1857466	1970016	1916086	1904997
SE	3033711	2595210	1425725	2255382	2413477	1921105	2421809	1921105	2421809	2237755	1888971	1705620
RO	1210776	749726	821016	554720	551504	554366	554366	554366	584574	805549	887453	710307
PT	885134	1035260	1004623	952552	868993	1068043	1068043	1068043	1068867	1162195	1071201	1205464
SK	368585	347300	216421	321622	311014	166078	166078	166078	172008	209550	216381	184395
SI	108426	164339	97797	154385	148286	63158	63158	63158	67995	79897	92066	83404
UK	2807173	2799435	2939257	2642822	2649184	2382976	2506557	2382976	2513820	2554887	2704190	2293089

## Appendix III: Total nights spent for 2012 on a monthly basis

NUTS_ID	Jan-12	Feb-12	Mar-12	Apr-12	May-12	Jun-12	Jul-12	Aug-12	Sep-12	Oct-12	Nov-12	Dec-12
AT	11686954	12694298	10003386	6396395	6135581	8276346	12669327	14446817	9007088	6052904	3861887	8309737
BE	1386362	1755803	2145579	2833613	2924419	2545434	4436023	4081007	2666508	2536373	2040269	1916051
BG	613539	572800	575232	656338	992912	3123432	4845940	4861004	2255812	650350	502653	602026
CZ	2601660	2808047	2995410	3160367	3684358	3849146	5935137	6037775	4044037	3281050	2475636	2405834
DE	17259651	18916243	22226883	27488029	33923648	34643820	42279467	44513846	36430512	31702181	20850437	20435788
DK	786116	935952	1403551	2192298	2958760	3076859	6309002	4087176	2245812	1491781	1222765	1330163
ES	17377536	19006446	22804233	27801602	30860605	39565705	54599312	62362414	41988326	30276552	18641630	17386615
EL	1097955	1018325	1435397	2508078	6649683	12050223	17760110	19771963	11782306	4298848	1067585	1126199
EE	322407	292770	358837	405218	476017	580976	818315	672105	426815	431665	368218	391194
FR	18264635	20445663	22939758	24629501	31396572	36788183	71222005	83996716	35051221	21425193	16479301	18213668
FI	1402874	1458832	1739878	1395247	1340572	2130407	3025894	2216899	1555183	1396297	1311438	1343611
IS	82194	122323	155819	149850	208760	448232	759229	643339	252341	165881	138524	105170
IT	15708685	15406926	18009007	23191731	27279007	44496843	69088155	79845672	40580654	21149301	12202027	13753475
HU	991859	963338	1298125	1642535	1868133	2307354	3575194	3874205	2087091	1809621	1377987	1267161
HR	298788	277416	548791	1608586	3213768	7525682	18333628	20544864	7383464	1657466	451203	340269
NO	1555785	1856462	2000244	1721933	2345986	3702028	5276579	4015450	2394685	1873217	1806665	1365283
ME	62247	51799	80744	125010	393052	965377	2375955	3611585	1222658	142121	72474	48214
MT	342961	395268	482518	629298	690546	799276	1010513	1021959	839089	767401	480432	372967
NL	3655827	3701137	4519843	7497626	9154943	8538213	11194669	13069998	7525671	6615182	4455672	4121624
LU	122499	130068	156938	205173	254267	261635	401304	356312	211129	189647	136328	118530
LI	11879	14983	11717	8695	10290	11380	15979	18124	12404	11377	5929	8285
LT	306556	271381	330493	351654	446184	558369	796796	744330	439981	372492	335009	312318
LV	215205	185731	209894	244427	293891	371243	506324	466493	297692	267410	245251	243175
PL	3534677	3645075	3743396	3995517	5340588	5822998	9434621	9163888	5807793	4592766	3633121	3300450
SE	2413354	2746735	3100791	2898712	4074424	5113101	10405576	6672995	3332666	2865763	2688245	2273610
RO	814623	693058	931758	1088270	1537552	1984938	2992546	3313110	1850724	1564533	1314956	1005311
PT	1766748	2107574	2804584	3525285	3888605	4694596	6422458	8292542	5430564	3809271	2191357	1847507
SK	656006	777247	727630	681222	869471	976505	1427483	1460952	1015471	872481	709439	596421
SI	576475	539178	551104	629785	679352	882902	1368706	1600943	842867	606570	488673	483897
UK	12048031	11561416	17607267	25527328	25712580	31195250	39382116	46404571	30792331	21862729	20132316	18123253

## Appendix IV: Total nights spent for 2013 on a monthly basis

NUTS_ID	Jan-13	Feb-13	Mar-13	Apr-13	May-13	Jun-13	Jul-13	Aug-13	Sep-13	Oct-13	Nov-13	Dec-13
AT	11423251	12949846	11405503	5060220	6462256	7880007	12909698	14922105	8841812	6157330	3942773	8732576
BE	1399318	1741163	2206858	2610945	2942541	2539341	4538718	4264029	2635746	2644382	2024140	1753220
BG	644094	667258	631977	583371	1183959	3466314	5027039	5024997	2386817	717568	602545	681535
CZ	2555690	2876204	3166229	2933205	3828516	3698657	5988439	6060660	3925324	3290806	2490709	2493840
DE	17522839	19109161	23680421	25070918	34737611	34070710	44328750	45844494	35928919	33122184	21625323	20766659
DK	817837	977179	1565038	1952359	2922122	3121491	6566071	4147508	2250488	1526010	1238269	1416465
ES	16507093	17778666	25276019	24384309	33427068	40475353	54757896	63578378	42582527	31578463	20112666	18753548
EL	1024556	995142	1461513	2293845	8193347	13873170	19280914	21397562	13099300	5143402	1175191	1167502
EE	336908	298781	380170	374968	496640	605871	834585	731521	439229	442513	390273	402574
FR	17839257	19831529	24461952	23057695	34478759	37361249	72109559	87171339	35114891	22204484	16027717	18424557
FI	1361168	1435794	1737710	1348645	1354692	2157050	3047325	2182636	1546195	1367479	1343040	1344059
IS	119717	187148	232087	191460	281014	586147	1006631	796271	313865	229130	178049	159166
IT	14703198	15205999	19097289	19883279	28948157	42707293	68500582	79652337	40286304	21486508	12299190	14015479
HU	995563	1031316	1463891	1546138	2158421	2397227	3928533	4089432	2107872	1894475	1476279	1337001
HR	266707	304120	672532	1451115	3794450	7674639	18705901	21266572	7625731	1777987	500120	378418
NO	1576456	1911758	2092942	1944263	2277385	3560324	5100884	3778106	2237943	1835819	1736440	1255205
ME	57059	53967	79580	127826	421689	1008774	2289333	3765533	1290797	185226	73270	58889
MT	372682	418983	542662	684558	802051	882081	1040561	1096029	891725	826393	543959	399464
NL	3803243	3988273	5084853	7261649	10878897	9516680	13250849	16380649	8796304	7532496	4989388	4590809
LU	134061	135858	174657	196049	284573	271395	418998	358755	206440	190537	146077	120081
LI	12186	14552	13982	7392	7928	10307	14443	17273	12114	11539	5828	7759
LT	328083	280777	360507	393371	550427	650197	872516	852597	536718	455009	422978	385876
LV	234981	200844	235772	248013	326183	396927	544876	519421	300866	279224	258330	229755
PL	3459662	3648722	3648561	3880741	5303001	6129169	9663322	9435863	5725735	4720895	3874698	3469083
SE	2357360	2658644	3081094	2810318	4219508	5276282	10823108	6890629	3404459	3029601	2832462	2326962
RO	859943	849844	882088	1030179	1434210	2059396	2866312	3304379	1901626	1588266	1423184	1097162
PT	1761303	2120446	3076245	3383804	4402613	5076553	6728902	8972805	5712703	4151000	2406546	2095339
SK	716861	841792	870943	746543	916827	1013975	1475723	1515277	985518	899096	741100	621986
SI	515873	540687	555048	555417	742268	863324	1415023	1633394	869891	631344	473655	484289
UK	12124968	14544036	20216293	22541951	28632988	31454717	43766768	48516385	31693672	25605059	17277395	16787771

## 9. AUTHOR INDEX

- B**  
Bansal, 36, 50
- C**  
Carlowicz, 19, 50  
Cazzolino, 21  
Chalkias, 36, 50, *See*  
Charlton, 36, 52  
Cinzano, 17, 50, 51  
Cozzolino, 50  
Croft, 13, 50
- D**  
Darlington, 33, 34, 50  
Doll, 11, 12, 15, 20, 50
- E**  
EC, 9, 27, 51, 52  
Elvidge, 11, 12, 13, 14, 15, 16, 20, 21, 22, 23, 28, 50, 51, 52, 53, 55, 56  
Eurostat, 10, 25, 26, 27, 52
- F**  
Fotheringham, 36, 45, 47, 52, *See*  
Fotis, 36
- G**  
Galimberti, 29, 52  
Ghosh, 15, 51, 52
- H**  
Hanwei, 22, 52  
Hattori, 22, 52  
Hayes, 33, 34, 50  
Henderson, 28  
Hsu, 22, 51, 52, 53, 56  
Huang, 13, 14, 17, 53, 54, 55
- I**  
Imhoff, 13, 14, 51, 53
- J**  
Jing, 20, 53
- K**  
Kaifang, 31, 53  
kalogirou, 36
- L**  
Lasta, 21, 50  
Letu, 16, 53  
Li, 31, 53, 55  
Liang. *See*  
Lu, 14, 53
- M**  
Meng, 20, 54  
Milaka, 36, 54  
Mukim, 10, 54  
Murack, 33
- N**  
NASA, 17, 19, 23, 53, 54  
NOAA, 18, 23, 51, 54
- O**  
OSCAR, 24, 54
- P**  
Palanga, 36
- R**  
Raupach, 20, 55  
Rayner, 17, 55
- S**  
Saitoh, 21, 55  
Scott, 17, 18, 19, 55  
Shi, 19, 20, 22, 55  
Small, 14, 51, 55  
Stathakis, 30, 55  
Stevenson, 27, 55  
Su, 20, 55  
Sutton, 15, 16, 51, 52, 55, 56
- U**  
UNWTO, 9, 27, 56
- W**  
Wei, 24, 56
- X**  
Xin, 31, 56
- Z**  
Zhang, 20, 28, 55, 56  
Zhao, 20, 32, 53, 56
- O**  
Ou, 20

**10. SUBJECT INDEX**

- A**  
 AIC, 36, 45  
 autocorrelation, 36, 39
- C**  
 calibration, 11, 12, 22, 23, 28, 51  
 clustered, 39, 45  
 correlation, 2, 10, 14, 16, 20, 25, 28, 34, 35, 37, 38, 39, 45, 46, 47, 48, 49
- D**  
 dependent variable, 14, 33, 34, 37, 39  
 dispersed, 39  
 DMSP, 2, 6, 7, 11, 12, 13, 14, 19, 20, 21, 22, 23, 24, 25, 26, 28, 30, 31, 34, 37, 39, 47, 49, 50, 51, 53, 54, 55, 56  
 DN, 19, 30
- E**  
 Europe, 2, 9, 24, 27, 28, 31, 37, 46, 47, 49  
 exponential smoothing, 20, 32
- F**  
 forecasted, 32, 49
- G**  
 GIS, 2, 50, 54, 55  
 GWR, 2, 6, 7, 28, 36, 45, 46, 47, 49, 52
- I**  
 image processing, 6, 28, 31, 32  
 independent variable, 33, 34, 39
- L**  
 LAEA, 28, 31  
 likelihood, 45  
 Linear regression, 2, 33
- M**  
 model, 7, 14, 15, 16, 29, 33, 36, 37, 38, 39, 47, 49  
 Moran's I, 36, 38, 47
- N**  
 night-lights, 50  
 night-time, 2, 6, 7, 10, 11, 12, 13, 15, 16, 19, 20, 21, 22, 24, 48, 49, 52, 53, 54, 55, 56
- O**  
 OLS, 2, 6, 7, 11, 12, 13, 14, 15, 16, 17, 19, 20, 21, 22, 23, 28, 30, 31, 33, 34, 36, 45, 47, 49, 51, 53, 54, 55, 56  
 outliers, 19, 36
- P**  
 pattern, 36, 38, 39, 45  
 Pearson, 34, 47  
 proxy, 10, 22, 27, 33  
 p-value, 39, 47
- R**  
 $R^2$ , 29, 37, 45, 46, 47  
 random, 13, 33, 38, 39, 45, 47  
 regression, 2, 6, 14, 15, 16, 20, 28, 29, 33, 34, 36, 37, 38, 41, 45, 47, 49, 50, 52, 54
- S**  
 scatterplots, 34, 36  
 seasonal, 0, 2, 10, 19, 25, 28, 34, 49  
 Seasonality, 48  
 SOL, 2, 6, 7, 25, 28, 30, 31, 33, 34, 37, 38, 39, 47, 48, 49, 57, 58  
 spatial, 9, 12, 14, 16, 17, 20, 22, 26, 36, 38, 39, 45, 47, 48, 49, 52, 54  
 spatial heterogeneity, 45
- T**  
 tourism, 2, 9, 10, 27, 33, 51
- V**  
 VIIRS, 2, 6, 7, 17, 18, 19, 20, 21, 22, 23, 24, 25, 28, 31, 32, 34, 37, 41, 46, 47, 49, 50, 51, 53, 54, 55, 56, 57, 58
- W**  
 WGS84, 28, 31
- Z**  
 zonal statistics, 30, 33  
 z-score, 39, 45